JOURNAL OF GEOPHYSICAL RESEARCH, VOL. 96, NO. D5, PAGES 9133-9157, MAY 20, 1991

Solar Radiative Line-by-Line Determination of Water Vapor Absorption and Water Cloud Extinction in Inhomogeneous Atmospheres

V. RAMASWAMY

Atmospheric and Oceanic Sciences Program, Princeton University, New Jersey

S. M. FREIDENREICH

NOAA Geophysical Fluid Dynamics Laboratory, Princeton, New Jersey

The complete available spectral features (line-by-line, or LBL) of the water vapor molecule in the solar spectrum and a precise treatment of particulate scattering are employed to obtain and analyze the solar radiative fluxes and heating rates in plane-parallel, vertically inhomogeneous model atmospheres containing vapor only, water cloud only, and vapor-plus-cloud present simultaneously. These studies are part of the Intercomparison of Radiation Codes in Climate Models (ICRCCM) project and constitute useful benchmark computations against which results from simpler radiation algorithms can be compared. The "exact" solution of the radiative transfer equation for cloudy atmospheres with the cloud in a single model layer consumes an exorbitant amount of computational resources (~100 hours on a Cyber 205). Two other techniques that are considerably more economical are also investigated. These techniques, too, are based on the LBL spectral features of the H_2O molecule but consist of an approximation in either the vapor optical depth or in the multiple-scattering process. The technique involving the "binning" of the vapor optical depths yields extremely accurate fluxes and heating rates for both the vapor and vapor-plus-cloud cases; in particular, it is a practical alternative for obtaining benchmark solutions to the solar radiative transfer in overcast atmospheres (3.8 hours). In contrast, the multiple-scattering approximation technique does not yield precise results; however, considering its computational efficiency (0.5 hours), it offers a rapid means to obtain a first-order approximation of the spectrally integrated quantities. The analyses of the alternate techniques suggest their potential use for high spectral resolution sensitivity studies of the radiative effects due to various types of clouds.

1. INTRODUCTION

Water substance in the Earth's atmosphere, in vapor, liquid, or solid phases, possesses distinctive optical properties in the solar spectrum. Scattering by the solid and liquid forms occurs throughout the spectrum, while absorption by all the phases occurs primarily in the near infrared. To evaluate the transfer of solar radiation for plane-parallel, horizontally homogeneous atmospheres on a theoretically precise basis [*Chandrasekhar*, 1950; page 9, equation (47)] the computations have to be performed at a sufficiently high spectral resolution, accounting for all of the fine features in the optical properties of the constituents. Further, for a vertically inhomogeneous atmosphere, adequate vertical spatial resolution is also required.

The absorption cross section of the water vapor molecule has a very fine structure [*Rothman et al.*, 1983] in the near-infrared spectrum. A precise calculation of the absorption of the direct beam by water vapor in a vertically inhomogeneous model atmosphere involves computing the transmission function (Beer's law of exponential attenuation) in each layer at ~3 million monochromatic frequencies. Such line-by-line (LBL) computations are cumbersome but not necessarily an enormous task. *Chou* [1986] has considered spectral resolutions as fine as 0.01 cm^{-1}; other investigations [*Kerschgens et al.*, 1978; *Wiscombe et al.*, 1984; *Kratz and Cess*, 1985] have employed wider intervals.

The condensed phase of H_2O, in contrast to the vapor form, exhibits properties that can be regarded as constant across wide spectral intervals (hundreds of wave numbers). Due to scattering of the direct beam into different directions by the particles, the presence of solid and liquid forms in any layer introduces a multiplicity of directions in the reflected and transmitted beams; one method for handling this interaction precisely in the case of plane-parallel clouds is the multiple-stream, doubling-adding (DA) method [*Hunt and Grant*, 1969], performed separately for each spectral interval. The computations for cloudy layers [e.g., *King and Harshvardhan*, 1986], although not as simple as the exponential attenuation of the monochromatic beams in the case of the vapor, do not pose any serious obstacles in terms of computer resources.

The most significant but computationally formidable problem arises when interactions with both water drops and water vapor have to be considered simultaneously. The task is rendered enormous because (1) the spectral resolution for the computation is determined by the finely varying absorption features of the water vapor molecule and (2) the presence of cloud drops requires consideration of the directional properties of the scatterers. For a precise solution, these two factors necessitate the employment of the DA method at each frequency point and applied to the inhomogeneous atmosphere (line-by-line plus doubling-adding, or LBL + DA computations). Since this places an excessive demand on the computational resources, investigations in the past have simplified the problem by employing wider frequency intervals and, in some instances, approximating the scattering by the particles [*Lacis and Hansen*, 1974; *Stephens*, 1978; *Kerschgens et al.*, 1978; *Liou and Wittman*, 1979; *Fouquart and Bonnel*, 1980; *Davies et al.*, 1984; *Wiscombe et al.*, 1984].

Paper number 90JD00083.
0148-0227/91/90JD-00083$05.00

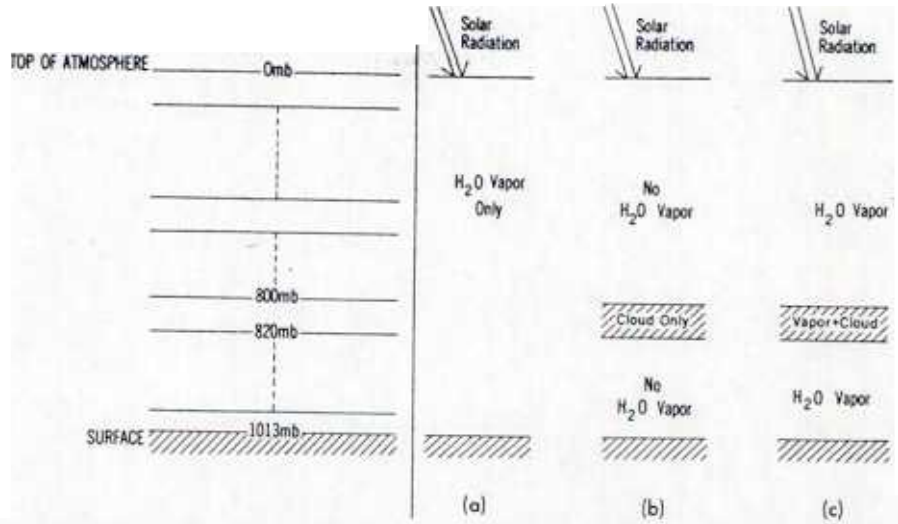

Fig. 1. Schematic description of the (*a*) vapor-only, (*b*) cloud-only, and (*c*) vapor-plus-cloud radiative transfer problems for a plane-parallel, vertically inhomogeneous atmosphere above a Lambertian reflecting surface. The model structure (section 2) is shown on the left. The cloud is located in the 800- to 820-mbar layer.

Despite the complexities, the need for a precise evaluation of the radiative fluxes and heating rates is paramount for quantifying the transfer in clear and cloudy atmospheres. The need is further reinforced by weather and climate model requirements of accurate parameterizations that have to be calibrated against the "exact" solutions. These are, in fact, the goals of the International Comparison of Radiation Codes for Climate Models (ICRCCM) project [*Luther et al.*, 1988]. Since practical considerations render the LBL + DA method prohibitive when several different cloudy atmosphere cases have to be considered, it is logical to inquire whether alternate economical techniques can provide highly accurate, benchmark quality results.

The main objective of this study is to determine precise radiative transfer solutions for plane-parallel vertically inhomogeneous atmospheres containing vapor only, cloud only, and vapor-plus-cloud present simultaneously (Figure 1). The input parameters adopted for the studies (section 2) are similar to those prescribed as part of the ICRCCM project.

To begin with, the calculation of the solar absorption by water vapor in a clear atmosphere is performed for different atmospheric profiles, using the LBL spectral features (section 3). Next, radiative properties of clouds of two different optical depths are evaluated (section 4) in an atmosphere containing no water vapor. This situation is of academic interest but serves as a useful intermediate study between the vapor-only and the vapor-plus-cloud cases.

Finally, the radiative transfer problem involving clouds and water vapor is investigated (section 5). Besides the exact (LBL + DA) method, more economical techniques, that approximate either the molecular absorption or the cloud extinction, are also employed. A summary of the techniques employed for the vapor-only, cloud-only and vapor-plus-cloud cases, along with their CPU times on the Cyber 205 computer, is listed in Table 1. Details about the techniques mentioned appear in the subsequent sections of the text.

2. Model and Data

Based on the atmospheric reference profiles of *McClatchey et al.* [1972] and the suggestion of a constant water vapor mixing ratio above the tropopause by the ICRCCM project, a model of the vertically inhomogeneous atmosphere is developed (Figure 1). The model spans the pressure levels from the top of the atmosphere (0 mbar) to the surface (~1013 mbar). Between zero and 1000 mbar there are 50 layers, each 20 mbar thick, while the lowest layer is 13 mbar thick. Properties are assumed to be uniform within each layer. The vertical resolution of the model is similar to that employed by *Chou* [1986]. The lth layer in the model is bounded by the lth and the $(l + 1)$th levels. The frequency interval considered in this study is 0–33,333 cm^{-1}.

2.1. *Molecular Absorption Properties*

The water vapor absorption spectra are taken from the line parameter compilations of the Air Force Geophysics Laboratory (AFGL) [*Rothman et al.*, 1983]. The precision of the location of the line center in the AFGL catalog is 0.01 cm^{-1}. Water vapor absorption lines extend from <1 to 17,900 cm^{-1}. The water vapor absorption optical depths are computed [see *Drayson*, 1973] according to the same algorithms as have been employed by *Schwarzkopf and Fels* [this issue] for developing benchmark calculations in the longwave spectrum. The procedure consists in dividing the spectrum into 1 cm^{-1} intervals, within each of which the absorption characteristics are represented by considering several discrete frequency points. The number of such monochromatic frequencies M_ν required within each wave number ν ($0 \leq \nu \leq 17{,}900$ cm^{-1}) is described by *Drayson* [1973].

The computation of absorption at each frequency point over the 1 cm^{-1} interval accounts for the fact that the tails of the lines extend out to 10 cm^{-1} beyond the line center; thus, any 1 cm^{-1} interval "perceives" the effect of lines whose centers are located up to 10 cm^{-1} away. At altitudes below 100 mbar, the absorption is computed based on a Lorentzian

TABLE 1 Summary of Techniques

Technique	Description	Nature of Approximation (If Any)	CPU Time hours
	Vapor Only		
Exact	LBL transfer; ~2.8 × 10^6 frequencies; 51 layers	—	
Binning	Range of vapor optical depth (10^{-12}– 10^2) in the atmosphere binned	Vapor absorption at each frequency in the atmosphere	
	Cloud Only (in One Layer)		
Exact	DA, 32-stream transfer; 107 distinct intervals in single-scattering properties	—	<0.01
Two stream	DE approximation in each interval	Cloud layer properties	<0.01
	Vapor Plus Cloud (in One Layer)		
VC1 (exact)	DA in the cloud layer; 32-stream transfer at ~2.8 × 10^6 frequencies	—	101
VC2	DE at each of ~2.8 × 10^6 frequencies	Cloud layer properties	0.50
VC3	Vapor optical depth range binned in cloud layer for each of 97 intervals in cloud properties; DA, 32-stream	Vapor absorption in cloud layer	3.80

Listed in the table are the main features of each technique and the CPU time (on Cyber 205) required to perform high spectral resolution computations of the solar radiative transfer in a 51-layer, plane-parallel, vertically inhomogeneous atmosphere containing water vapor only, cloud only, and water vapor plus cloud; the results of the investigations are discussed in sections 3, 4, and 5, respectively. The CL cloud is located in the 800- to 820-mbar layer, and the cloud-related cases pertain to an optical depth of 9.7 at a wavelength of 0.55 μm.

line profile. Above 100 mbar, a Voigt profile is assumed for distances less than 3 cm^{-1} away from the line center; for larger distances, again a Lorentzian profile is assumed.

According to the above prescription, each 1 cm^{-1} interval requires at least 40 points for representation of the absorption characteristics over that interval. Because of the use of a quadrature scheme, each frequency point i in a wave number interval has a definite weight (w_i); the weights are normalized to unity within each interval.

The greater the number of lines in any 1 cm^{-1} interval, the more the number of points needed to represent the absorption effects in that interval, e.g., in strongly absorbing spectral regions, more than 200 discrete points are required to represent the absorption features. The procedure described is performed for each wave number in the AFGL catalog. This ensures a very high spectral resolution for all the layers in the inhomogeneous atmosphere and thus facilitates a precise theoretical calculation, one that has not been attempted thus far in the literature for the near-infrared spectral regions.

The above formalism yields absorption optical depths (τ_i, l) at the ith discrete frequency in any wave number interval for the lth layer. The layer optical depths, for present purposes, range from 0 to 100 in the inhomogeneous model atmosphere. The number of monochromatic frequencies is ~2.8 × 10^6 (average spectral resolution ~6 × 10^{-3} cm^{-1}), so that in the problem involving only the absorption of the direct beam by water vapor, about (2.8 × 10^6)51 transmissions have to be computed (~1.4 × 10^8 exponential operations).

Cloud Optical Properties

the frequency interval from 0 to 33,333 cm^{-1}. In contrast to the rapid variation of water vapor absorption with frequency, the properties of droplets are relatively uniform over broad frequency intervals. The ICRCCM compilations of the single-scattering properties (extinction coefficient, single-scattering albedo, and asymmetry factor) list values at 107 distinct frequencies in the entire solar spectrum.

Clouds are assumed to be homogeneous and plane parallel, being confined to a single model layer (800–820 mbar; ~2-km altitude) in this study. At any frequency, the computation of the radiative properties of any layer in which scatterers are present is performed in two ways. The first is the multistream, doubling-adding (DA) technique, as described by *Hunt and Grant* [1969], and using the infinitesimal generator initialization scheme described by *Wiscombe* [1976]. We have investigated the results of using different streams (8–128 over the angular range 0–90°) for the radiative transfer in a layer containing cloud and vapor. Computations with 32 streams (based on a Gauss quadrature scheme) differ negligibly from those employing more streams; hence, for present purposes, 32 streams are deemed to resolve adequately the angular dependence of the radiation fields. The initial optical depth for the doubling calculations has a nominal value of 10^{-6}. The stringent choice of the parameter values above is dictated by the need to avoid even small inaccuracies at any monochromatic frequency point which can jeopardize the overall accuracy of the sum over several such points (e.g., entire spectrum).

Single-scattering properties at each frequency are specified based on the CL cloud specifications of the ICRCCM. At frequencies intermediate to those tabulated, the mean value of the parameter is assumed to be the representative value in that interval. The asymmetry factor is used to obtain the Henyey-Greenstein phase function [*Hansen and Travis*, 1974]. This is a smoothly varying phase function in contrast to the Mie phase function [*King and Harshvardhan*, 1986] for clouds. The Henyey-Greenstein phase function is expanded into a 64-term (an optimum value) Legendre polynomial set to represent the anisotropic scattering by the liquid drops at each frequency. As has been noted in several earlier investigations, the cloud single-scattering properties imply absorption at frequencies below 18,000 cm^{-1}; the single-scattering albedo increases with increasing frequency, even-

tually leading to (for pure water drops) scattering only beyond 18,000 cm^{-1}. The extinction optical depth is relatively uniform for $\nu > 1000$ cm^{-1} across the spectrum, varying within 14% of the value at $\lambda = 0.55$ μm (~18,182 cm^{-1}). The asymmetry factor, too, does not vary by more than 13% between 1000 and 33,333 cm^{-1}. Results using the DA technique have been compared with the case studies tabulated by *Lenoble* [1977].

The second method considered for the scattering-absorbing problem is the delta-Eddington (DE) algorithm described by *Joseph et al.* [1976]. This method yields reasonably accurate radiative transfer results for thick clouds and is beginning to be employed in climate models [*Charlock and Ramanathan*, 1985; *Harshvardhan et al.*, 1987]. The wavelength-dependent single-scattering properties employed are the same as mentioned above.

It is pointed out that cloud optical depth at a wavelength of 0.55 μm is considered to be the reference value; cloud extinction optical depths are varied in this study by scaling the variations at all other wavelengths with respect to that at 0.55 μm. The current study considers optical depths of 1.0 and 9.7.

2.3. *Solar Irradiance Data*

The solar irradiance for either the study of water vapor absorption only, or for the cloud extinction, or for the case of water vapor absorption plus cloud extinction is prescribed according to the ICRCCM tables and follows *Labs and Neckel* [1970].

2.4. *Other Details*

The input parameters used in the experiments discussed below are, for the most part, those specified by the ICRCCM project. Thus the solar zenith angle considered for the calculations here is either 30° or 75°. Because of the employment of a quadrature scheme for the DA computations, the cloud-related results for the larger zenith angle pertain to a value of 75.7° This has a negligible effect on the discussions in this paper.

Water vapor absorption only calculations are performed with a surface albedo of zero (direct beam only) and 0.2 (Lambertian surface, as specified for the ICRCCM cases). The calculations with water drops assume the surface albedo to be zero. These assumptions have been made in order to study simple cases. Effects due to other gases like O_2, O_3, and CO_2 are also not considered in this study.

The cloud optical depth of 1.0 is a departure from ICRCCM specifications. This is in order to provide a contrast to the value of 9.7; at the same time, it is not too small so as to make a negligible difference in the radiative transfer relative to the vapor-only case.

The computational results are divided into those for the H_2O absorbing intervals (0–18,000 cm^{-1}) and that for the nonabsorbing interval (18,000–33,333 cm^{-1}). Within the absorbing frequency intervals, the results have been subdivided into 10 bands (Table 2). The mean frequency in each band and the corresponding wavelength are also tabulated. The limits of each band follow earlier works [e.g., *Kratz and Cess*, 1985] and, although arbitrary, are introduced here to facilitate the analyses. In Figure 2 the solar irradiance (W/m^2) in each of the absorbing bands as well as that in the nonabsorbing interval are illustrated for zenith angles of 30° and 75°. Note that the flux at the top of the atmosphere is nearly uniform in each band between 4 and 9 and then increases in bands 10 and 11.

TABLE 2. Frequency Intervals Covered by the Different Bands Used for the Study of Solar Radiative Transfer

Band Number	Frequency Interval, cm^{-1}	Mean Frequency, cm^{-1}	Mean Wavelength, μm
1	0–1,000	500	20.00
2	1,000–2,500	1,750	5.70
3	2,500–4,400	3,450	2.90
4	4,400–6,200	5,300	1.89
5	6,200–8,200	7,200	1.39
6	8,200–9,700	8,950	1.12
7	9,700–11,500	10,600	0.94
8	11,500–13,000	12,250	0.82
9	13,000–14,500	13,750	0.73
10	14,500–18,000	16,250	0.62
11	18,000–33,333	25,667	0.39

The mean frequency within each interval and the corresponding wavelength (μm) are also listed.

The results are arranged in two distinct ways as follows: (1) results from the exact method and (2) comparisons of the results from the approximate methods with those from the exact. Departures from the exact values are evaluated either in terms of the relative error (δ_{re}), defined as

$$\text{(approximate} - \text{exact)/(exact)}$$

or in terms of its magnitude.

3. WATER VAPOR ABSORPTION

3.1. *Exact Method*

The transmission at any frequency point i within any wave number interval (the notation for the interval is suppressed) in any layer l is given by

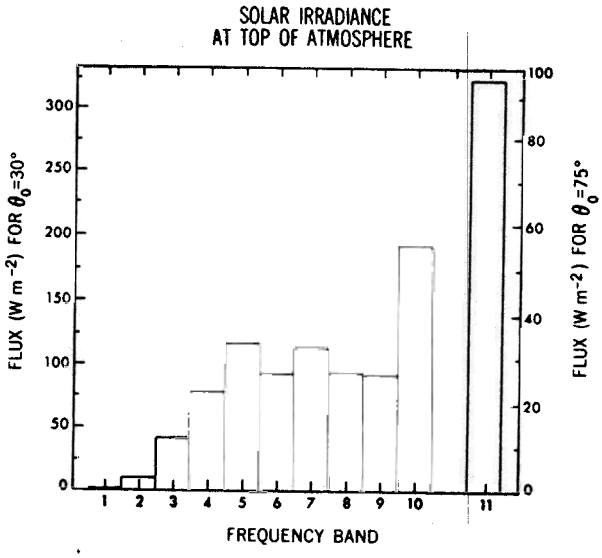

Fig. 2. Band-by-band (see Table 2) solar irradiance [*Labs and Neckel*, 1970] at the top of the atmosphere for solar zenith angles (θ_0) of 30° and 75°. Band 11, where vapor and cloud are nonabsorbing, is shown separated from the absorbing bands.

$$T_{i,l} = \exp\left[-(\tau_{i,l})/\mu_0\right] = \exp\left[-(q\Delta p\sigma_{i,l})/g\mu_0\right] \quad (1)$$

where q is the water vapor mixing ratio, Δp the layer pressure thickness, σ the vapor absorption coefficient, g the acceleration due to gravity, and μ_0 the cosine of the solar zenith angle (θ_0). The downward flux at any level L and at any frequency point is

$$F_{i,l}^{\downarrow} = \prod_{l=1}^{L-1} F_{0i}T_{i,l} \quad (2)$$

where F_{0i} is the incident irradiance at the top of the atmosphere at the concerned frequency point.

For a Lambertian reflecting surface with an albedo α, there is an upward diffuse beam at the surface,

$$F_{i,\mathrm{sfc}}^{\uparrow} = \alpha F_{i,\mathrm{sfc}}^{\downarrow} \quad (3)$$

The resulting upward flux at level L is

$$F_{i,L}^{\uparrow} = F_{i,\mathrm{sfc}}^{\uparrow} \prod_{l=L+1}^{51} T_{i,l}^{*} \quad (4)$$

where T^* denotes a diffuse transmission. T^* is evaluated by a four-point quadrature. The net flux at level L is

$$F_{i,L}^{\mathrm{net}} = F_{i,L}^{\downarrow} - F_{i,L}^{\uparrow} \quad (5)$$

while the heating rate in layer L is

$$Q_{i,L} = g(F_{i,L}^{\mathrm{net}} - F_{i,L+1}^{\mathrm{net}})/c_p\Delta p \quad (6)$$

where c_p is specific heat at constant pressure.

The total flux (downward, upward, or net) in the νth wave number interval comprised of M_ν discrete frequencies is

$$\sum_{i=1}^{M_\nu} F_{i,L}w_i \quad (7)$$

with w_i being the weight for the ith frequency.

The fluxes for the entire spectrum (18,000 wave number intervals) are given by

$$F_L = \sum_{\nu=1}^{18{,}000} \sum_{i=1}^{M_\nu} F_{i,L}w_i \quad (8)$$

while the heating rate is given by

$$Q_L = \sum_{\nu=1}^{18{,}000} \sum_{i=1}^{M_\nu} Q_{i,L}w_i \quad (9)$$

The exact calculation for a water vapor-only atmosphere (Figure 1*a*) is performed for all five *McClatchey et al.* [1972] profiles shown in Figure 3; these include the first six ICRCCM shortwave cases. The vertical distribution of the heating rates in the five atmospheres is shown in Figure 4. The surface albedo is 0.2 while zenith angles of 30° (Figure 4*a*) and 75° (Figure 4*b*) are considered. Note that calculations for clear sky have been performed earlier by *Chou* [1986] using a slightly coarser resolution in frequency space. Comparisons with M. D. Chou's (personal communication, 1989) results for the mid-latitude summer atmosphere indicate that the tropospheric solar heating rates from the two calculations differ by <1%.

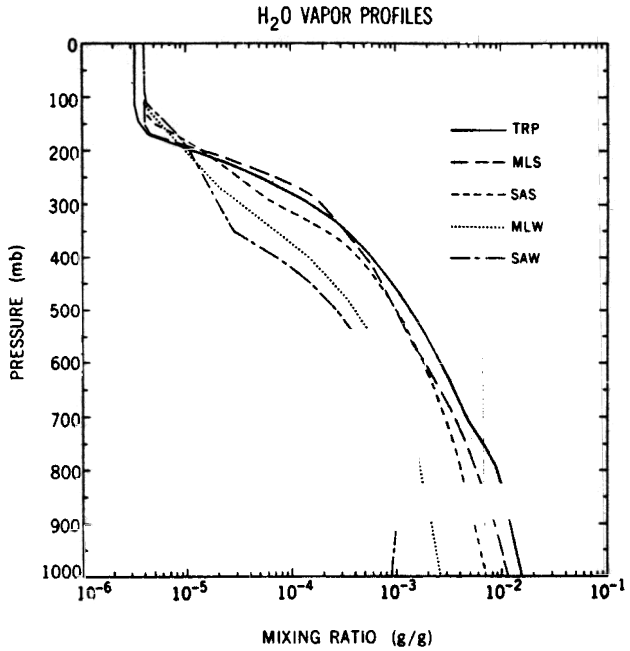

Fig. 3. Vertical profile of the water vapor mixing ratio [*McClatchey et al.*, 1972] for five different model atmospheres. TRP, tropical; MLS, mid-latitude summer; SAS, sub-Arctic summer; MLW, mid-latitude winter; and SAW, sub-Arctic winter.

The tropics, since they contain more vapor in the troposphere than any other profile, have the maximum heating in the middle and lower troposphere with the peak occurring at ~790 mbar. Again, because the tropics have less water vapor for $P < 200$ mbar, the absorption there is less. All profiles indicate a maximum in the heating between 300 and 800 mbar, with the peak shifted to lower pressure levels for the larger zenith angle. For $\theta_0 = 30°$, all profiles except the sub-Arctic winter (SAW) exhibit an increase in the lowest few layers.

For the upper troposphere in general ($P < 300$ mbar), the increase of water vapor with increasing pressure (Figure 3) results in an obvious increase in the heating rate. In the lower and middle troposphere the linkages are less evident, and the increase of the vapor mixing ratio with pressure is not necessarily accompanied by an increase in the heating; in fact, there can actually be a decrease (e.g., all profiles at 75°) which is large for the SAW profile. This is due to saturation effects occurring in some of the absorbing frequencies so that fewer photons are available for absorption in the lower layers. The increase in heating seen for the lowermost layers (30°) is due to the absorption of the beam reflected at the surface. Yet another reason for the breaks in the heating rate profile is due to the change in the vertical gradient of the mixing ratio, e.g., the discontinuity at ~750–790 mbar in the tropical (TRP) profile (Figure 3) results in a peak in the heating rate curve (Figure 4).

Figure 5 illustrates the contribution to the vertical profile of the heating rate in the mid-latitude summer (MLS) atmosphere by the different bands (Table 2) for $\theta_0 = 30°$. The relative contributions to the heating in the 800- to 820-mbar layer (the choice of this layer is to facilitate comparisons with cloud-induced heating later on) from the different bands

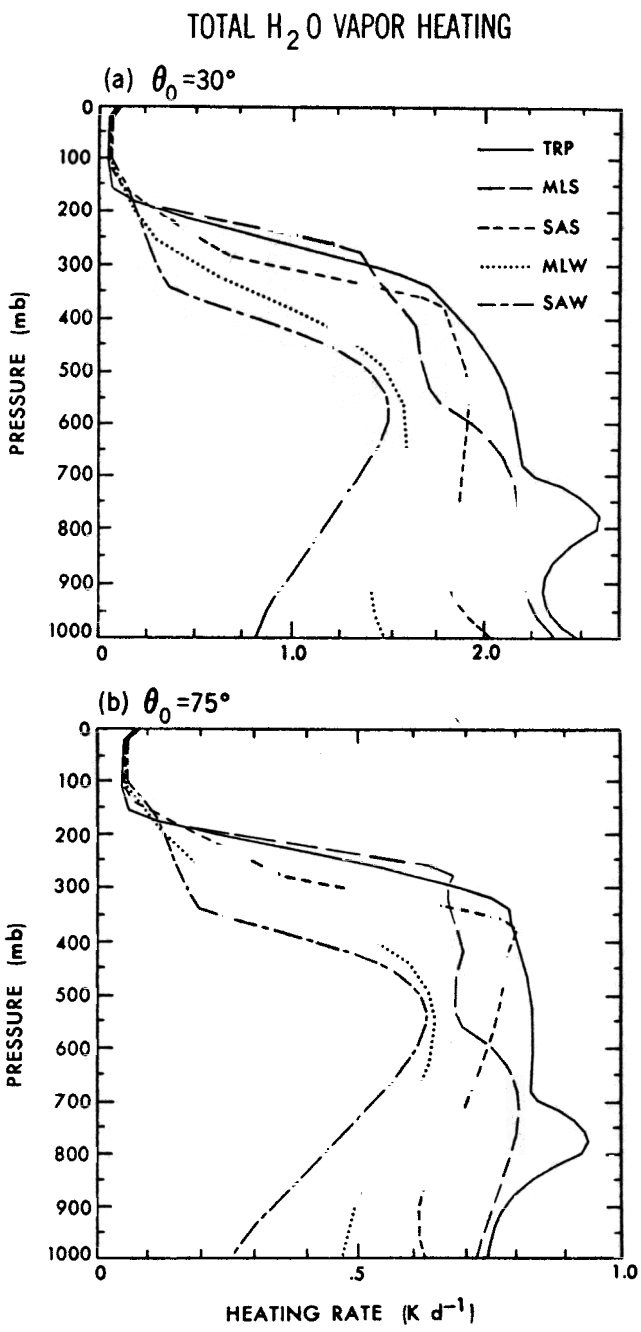

Fig. 4. Vertical distribution of the exact heating rate for five atmospheric profiles due to absorption of solar radiation by water vapor. Surface albedo is 0.2, while zenith angles (θ_0) of (*a*) 30° and (*b*) 75° are considered. TRP tropical; MLS, mid-latitude summer; SAS, sub-Arctic summer; MLW, mid-latitude winter; and SAW, sub-Arctic winter.

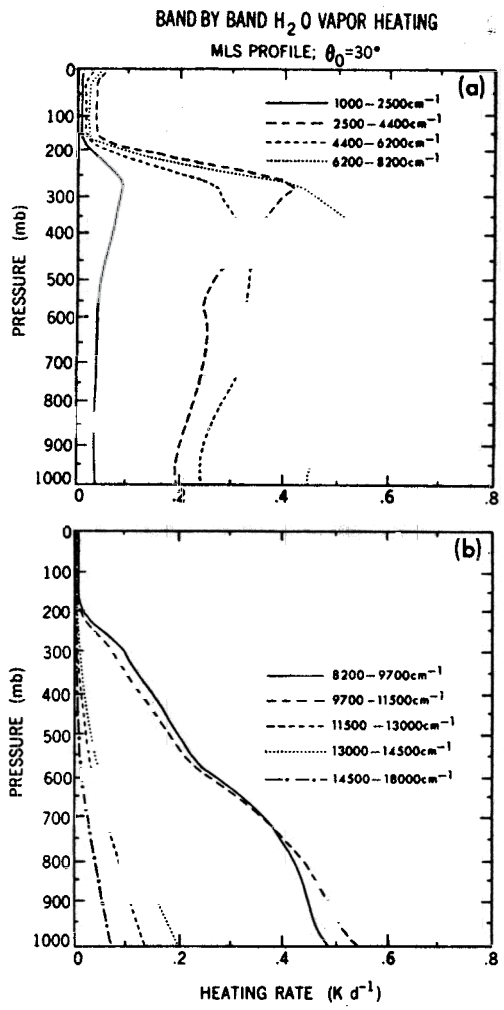

Fig. 5. Band-by-band contribution to the vertical distribution of the exact heating rate in the MLS atmosphere (zenith angle θ_0=30°) due to absorption of solar radiation by water vapor for frequencies (*a*) <8200 cm^{-1} and (*b*) >8200 cm^{-1}.

are listed in Table 3 for the direct beam. The major contribution to the heating in the upper troposphere (P < 300 mbar) arises from the 2500–8200 cm^{-1} interval, while bands between 2500 and 11,500 cm^{-1} are the major contributors in the middle and lower troposphere. Bands below 8200 cm^{-1} are partially saturated for P < 700 mbar, so that layer absorption decreases with increasing depth in the atmosphere; the remaining bands are unsaturated, and absorption increases with pressure.

Figure 6 is a similar illustration for θ_0 = 75°. The difference with respect to Figure 5 is that, for any altitude, there is an increase in the photon path lengths as measured from the top of the atmosphere; this causes bands to saturate partially at altitudes higher than for the 30° case. In fact, for θ_0 = 75°, even the 8200–9700 and the 9700–11,500 cm^{-1} bands are partially saturated in the lower troposphere (~730–750 mbar). Less solar flux is incident at the top of the atmosphere when θ_0 = 75°; this causes the magnitudes of the heating rates to be smaller than for the 30° incidence. The relative contribution to the 800- to 820-mbar layer heating at 75° is similar to or smaller than at 30° in bands 1–5 while being greater in bands 6–10 (Table 3).

The morphology of the water vapor profile in an inhomogeneous atmosphere affects the manner in which the solar direct beam is attenuated as it traverses the various layers. Because of the spectrally varying absorption properties, there will be a spectrally varying attenuation of the radiation at any level. In the present model, since each layer is of equal pressure thickness, three factors determine the heating in layers. The first is the attenuation at any frequency up to the layer in question. The second is the layer pressure, which determines the absorption characteristics of the mol-

TABLE 3. Total Heating Rate in the Solar Spectrum and the Contribution (in Percent) of Each Band to Heating in the 800- to 820-mbar Layer of an MLS Profile for Vapor Only, Cloud (Located in the Concerned Layer) Only, and Vapor and Cloud Together in the Atmosphere

		τ (cloud) = 1.0		τ (cloud) = 9.7	
Band, cm	Vapor	Cloud	Vapor Plus Cloud	Cloud	Vapor Pl Cloud
		$\theta_0 = 30°$			
0–1,000	0.2	1.3	1.3	0.5	0.6
1,000–2,500	1.6	14.3	11.2	7.1	6.2
2,500–4,400	10.3	47.7	29.1	28.4	20.2
4,400–6,200	12.7	23.4	24.0	32.9	33.8
6,200–8,200	25.5	11.7	17.8	26.5	28.4
8,200–9,700	19.3	1.3	7.2	3.4	6.3
9,700–11,500	19.9	0.3	6.2	1.1	3.3
11,500–13,000	3.6	0	1.1	0.1	0.5
13,000–14,500	5.4	0	1.6	0	0.6
14,500–18,000	1.5	0	0.5	0	0.2
Solar heating rate, K/d	2.05	11.58	8.38	56.85	37.35
		$\theta_0 = 75°$			
0–1,000	0.1	1.0	1.2	0.6	0.7
1,000–2,500	1.5	12.5	11.6	7.7	7.3
2,500–4,400	8.2	45.2	26.2	30.8	19.9
4,400–6,200	10.3	25.5	29.0	31.6	35.5
6,200–8,200	18.6	13.7	17.8	24.9	27.5
8,200–9,700	20.3	1.6	5.9	3.2	5.6
9,700–11,500	22.8	0.4	4.7	1.0	2.5
11,500–13,000	6.0	0	1.2	0.1	0.4
13,000–14,500	8.8	0	1.7	0	0.5
14,500–18,000	3.4	0	0.7	0	0.2
Solar heating rate, K/d	0.77	6.76	3.57	13.51	7.15

Cloud optical depths τ(cloud) of 1.0 and 9.7 (at a reference wavelength of 0.55 μm) and solar zenith angles (θ_0) of 30° and 75° (75.7° for the cloud-related cases) are considered. Surface albedo is zero. Zeros in column denote values <0.05%.

ecule at the concerned frequency. The third is the absorber amount in the layer.

To delineate these effects in different portions of the spectrum in the upper, middle, and lower troposphere, the contribution of each spectral band to the heating in the 180- to 200-, 580- to 600-, and 800- to 820-mbar layers is plotted in Figure 7 for solar zenith angles of 30° (Figure 7*a*) and 75° (Figure 7*b*). The 180- to 200-mbar layer is heated by absorption in the 1000–11,500 cm^{-1} interval (bands 2–7), while the other two layers are heated by absorption in bands 2–10. Figures 5 and 6 have already shown that saturation effects occur at bands <7. This becomes clearer in Figure 7, where it is seen that the heating in the 580- to 600-mbar layer exceeds that in the 800- to 820-mbar layer for the first five bands, while in the other bands, the situation is reversed. This feature has implications for the degree of absorption that can be introduced by water drops at different altitudes in the atmosphere. Water drop absorption (as will be seen later) has a frequency dependence similar to that for the molecule, so that if any of the bands are saturated due to water vapor absorption before the irradiance in that band can reach the cloud level, there will be little absorption by the cloud despite a high droplet absorption efficiency [*Davies et al.*, 1984]. This is an important issue for clouds located lower in altitude (e.g., absorption by stratus clouds in an otherwise clear atmosphere). Heating in the 180- to 200-mbar layer for any band is smaller than that in the 580- to 600-mbar layer, emphasizing the absence of saturation effects at $P < 190$ mbar.

Comparing the absorption resulting from the propagation of the direct beam and that due to the diffuse beam after reflection at the relatively low Lambertian surface (albedo 0.2), it is seen that the direct beam absorption contributes in a predominant manner to the total atmospheric absorption, being 94% for $\theta_0 = 30°$ and 98% for $\theta_0 = 75°$. The contribution by the reflected beam to the heating rate (Figure 8) becomes apparent only below the middle troposphere for an albedo of 0.2. While the contribution of the direct beam to the absorption above 800 mbar exceeds 95%, and is more so when the path length is longer (75°), the reflected beam's contribution assumes significance in the lowest few layers (up to 25% for 30°).

The downward flux at the surface (Table 4) is comprised principally of radiation in the nonabsorbing (>30%) and the weakly absorbing (~20%) bands (11 and 10), together with roughly similar contributions (~5–10%) from all bands 4–9. The frequencies in which water vapor exhibits strong absorption comprise ~65% of the surface solar flux.

Fouquart et al. [this issue] present detailed discussions of the absorption of solar radiation by water vapor from various algorithms, including Chou's and the present LBL calculations. It is important to mention that the present LBL calculations include three spectral regions that were not considered by *Chou* [1986]: 0–1000, 1000–2600, and 14,500–

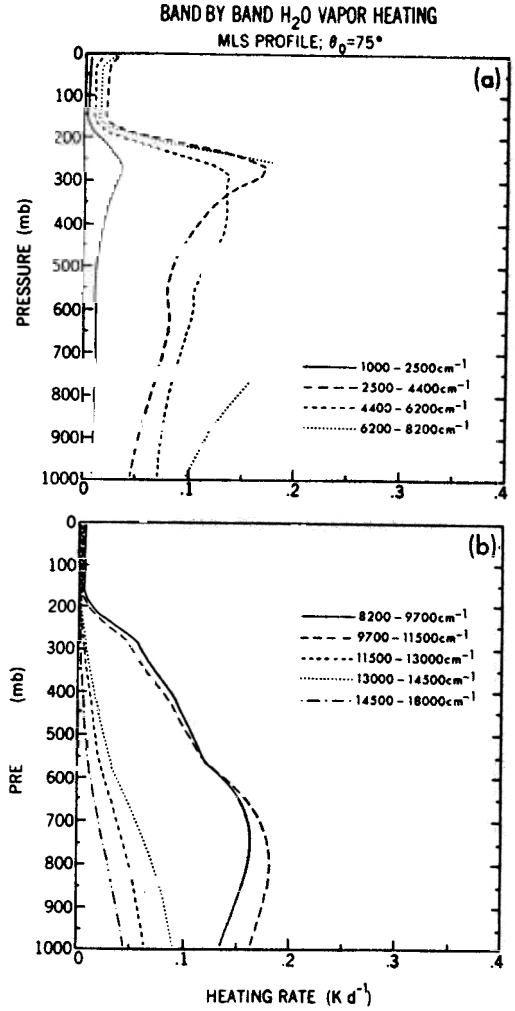

Same as Figure 5, execpt for solar zenith angle θ_0=75°.

18,000 cm^{-1}. The first two regimes have a small value of solar irradiance associated with them, while the third is weakly absorbing (Figures 5 and 6). The transfer of radiation in these regimes enhances the MLS atmospheric absorption (mainly in the 1000–2600 cm^{-1} regime) by 7.3 W/m^2 for θ_0 = 30° and by 3.3 W/m^2 for θ_0 = 75°; correspondingly, the surface flux decreases by a similar amount. The underestimate in the atmospheric absorption due to neglect of these regimes is 4.3% and 4.8%, for the two zenith angles, respectively; the corresponding overestimates in the surface flux are 1.1% and 1.8%, respectively. The total heating in any layer, however, is not measurably affected by neglecting these intervals.

3.2. *Binning Method*

From the computational viewpoint, a high-resolution calculation, as described above, involves the calculation of a large number of exponential functions. Although the time taken to perform the LBL computations is affordable (Table 1), it is worthwhile inquiring whether simplifications of the problem are possible without a loss of accuracy. For example, do the results remain unchanged when the number of the transmission computations is reduced, either through a coarsening in spectral interval (as investigated by *Chou* [1986]) or through a "binning" process as described below?

The binning technique, just like the exact technique, considers all the monochromatic frequency points (section 2.1); however, the vapor absorption optical depths are now partitioned into "bins" (or intervals). For practical purposes, it is sufficient to consider a lower limit of 10^{-12} for the vapor optical depth; smaller values are assumed to be zero and are placed in a bin which is denoted as the zeroth bin. The features of the binning procedure are summarized in Table 5. The range between 10^{-12} and 10^2 is binned such that there are an equal number of intervals (N) within each decade in optical depth, i.e., N intervals between 10^{-12} and

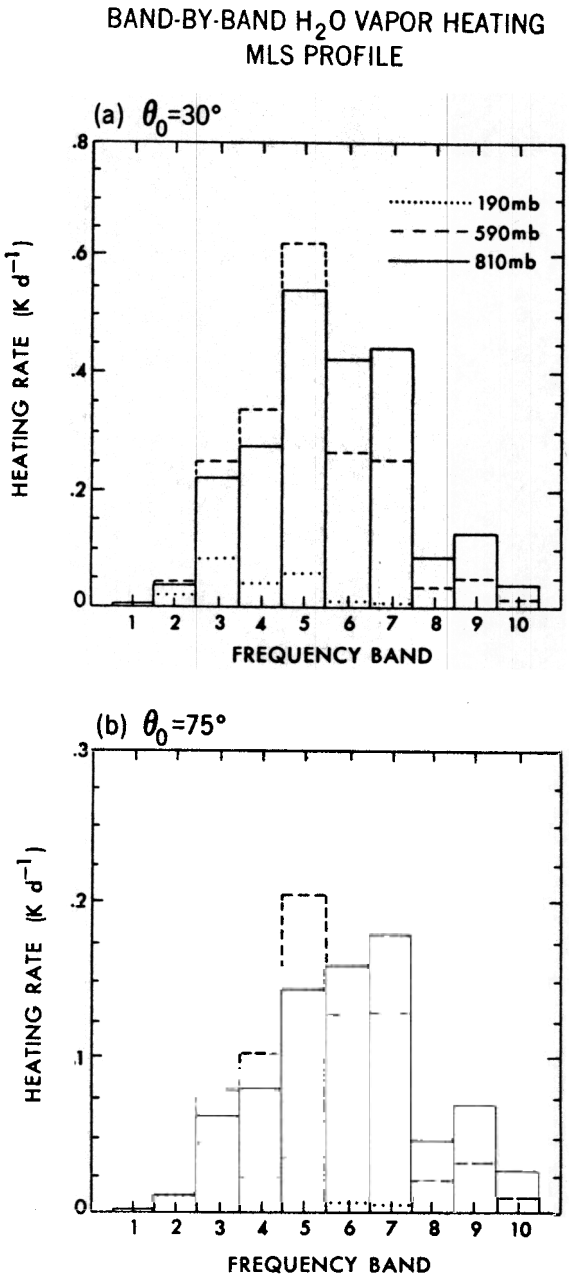

Fig. 7. Band-by-band contribution to the exact heating rate due to absorption of solar radiation by water vapor in the 180- to 200-, 580- to 600-, and 800- to 820-mbar layers of the MLS atmosphere. Zenith angle θ_0 is (*a*) 30^0 and (*b*) 75°.

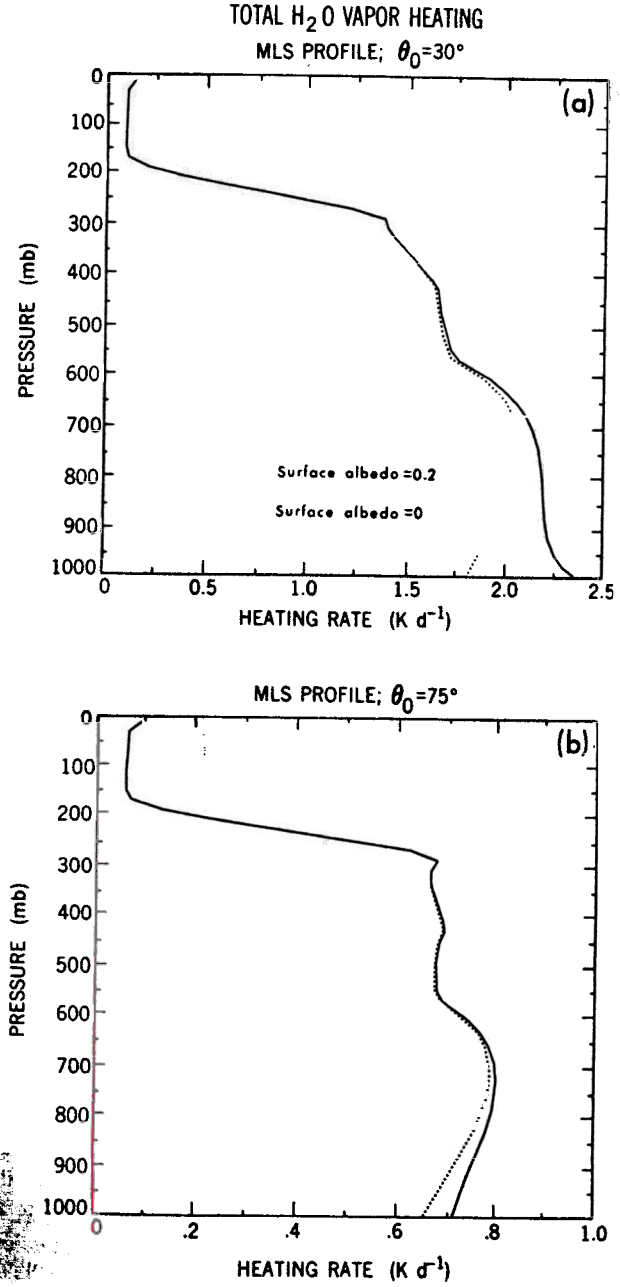

Fig. 8. Solar (exact) heating rate due to water vapor absorption for surface albedos of 0.2 and zero (direct beam absorption). Solar zenith angle θ_0 is (*a*) 30° and (*b*) 75°.

10^{-11}, N more between 10^{-11} and 10^{-10}, and so on till 10^2. The midpoint of any individual bin is assumed to be representative of all the optical depth values within the range of that bin. Thus the actual optical depth τ appearing in (1)–(9) is replaced by an appropriate bin value τ'.

Since the molecular absorption optical depth is assumed to span 14 decades in the model atmosphere, there are $14N$ intervals over the entire range of the absorption optical depth; in each of these, the transmission function is precomputed based on the value of τ'. The total number of τ' resulting from the binning process, or the transmission functions to be computed, is thus $14N$, i.e., each frequency point in any layer is represented by one of the $14N$ values of the transmission functions. Recalling that $\sim 1.4 \times 10^8$ transmission calculations are required for the exact transfer, it is evident that N can be chosen such that the number of the transmission computations is scaled down substantially.

It is instructive to examine the potential effects of binning on the absorption and transmission of radiation. Consider first a homogeneous layer and the discrete frequency points. The relative error in absorptivity arises due to the difference in the values of the optical depth between the exact and the binned values. It is easily seen that the magnitude of the error attains its maximum value for the first interval in each decade of the binning process, e.g., it is equal to 50% for $N = 9$, 5% for $N = 90$, and 0.5% for $N = 900$ (last column of Table 5). N is thus an arbitrary parameter governing the precision with which the specific value of the absorption optical depth at any frequency point is represented. In an inhomogeneous atmosphere, the binning process presents another source of error due to differences in the amount of radiation transmitted. For a layer well within the atmosphere, the incident radiation at the top of the layer can be in error, owing to differences in optical depth between the bin and the exact methods for all or a few of the layers above the one in question. The maximum relative error due to the differences in transmission can be large (>100%) for small absolute values, e.g., due to large optical paths through the atmosphere. Hence large relative errors could occur in the heating rate at any frequency point for layers within an inhomogeneous atmosphere. The absolute error, however, need not necessarily be large.

We have investigated the effects due to various values of the accuracy parameter $N = 900$, 90, and 9 bins per decade, respectively. This corresponds to 12,600, 1260, and 126 transfer computations, respectively, across the range of optical depths encountered in the inhomogeneous atmosphere and over the entire spectrum. The magnitude of the maximum relative errors in the heating rates ($|\delta_{re}Q|$) occurring anywhere over any band and over the solar spectrum for 30° and 75° solar incidences are listed in Table 6. The choice of examining the maximum relative error provides a stringent criterion for investigating the accuracy of the technique.

In general, the magnitude of the relative error becomes smaller as N is increased. For both zenith angles, there is more than an order of magnitude decrease in the relative error over any band and over the entire spectrum, when N increases from 9 to 90. A further reduction of about an order of magnitude or more occurs when N is increased to 900. Errors in any band for $N = 90$ are <0.1%, while those for $N = 9$ are <5%. The errors in heating rate for $N = 90$ are <0.04%, and for $N = 9$ are <2.5%. The magnitude of the relative error in the fluxes over any band for the $N = 90$ and 9 cases are less than 0.01% and 1%, respectively (Table 6). Over the entire spectrum, the errors are less than 0.004% and ~0.3%, respectively.

The flux and heating rates from the binning method are remarkably accurate. Although the relative errors are somewhat larger when $N = 9$, they occur in the upper troposphere where the absolute values are small. The excellent agreement with the exact values for the bin cases is pleasantly surprising, particularly when the wide disparity in the accuracy with which the absorption values are represented in the bin cases (Table 5) is considered; this suggests that approximate values of the water vapor absorption optical depth at the different frequency points may be adequate to compute the radiative effects due to water vapor absorption.

TABLE 4. Contribution (in Percent) From Each Band to the Total Downward Solar Flux at the Surface (F_{sfc}) and the Reflected Flux at the Top of the Atmosphere (F_{TOA}) in the 0–33,333 cm^{-1} Spectrum for the Vapor-Only, Cloud-Only, and Vapor-Plus-Cloud Cases

Band, cm^{-1}	Vapor Only	τ (cloud) = 1.0				τ (cloud) = 9.7			
		Cloud Only		Vapor Plus Cloud		Cloud Only		Vapor Plus Cloud	
	F_{sfc}	F_{sfc}	F_{TOA}	F_{sfc}	F_{TOA}	F_{sfc}	F_{TOA}	F_{sfc}	F_{TOA}
				$\theta_0 = 30°$					
0–1,000	0.1	0	0	0	0	0	0	0	0
1,000–2,500	0.5	0.5	0.3	0.3	0.2	0	0.1	0	0
2,500–4,400	1.6	2.6	1.5	1.2	1.0	0.2	0.5	0.2	0.4
4,400–6,200	5.3	6.4	6.7	4.9	5.3	2.9	4.0	2.2	3.3
6,200–8,200	6.8	10.0	10.7	6.6	7.2	7.3	8.6	4.6	5.7
8,200–9,700	6.9	8.1	9.0	6.8	7.6	8.2	9.1	6.4	7.6
9,700–11,500	9.0	10.0	10.6	9.0	9.6	10.6	11.4	9.0	10.1
11,500–13,000	9.1	8.3	8.3	9.2	9.1	9.1	9.3	9.7	9.9
13,000–14,500	8.7	8.1	8.0	8.8	8.6	9.0	9.0	9.2	9.4
14,500–18,000	19.3	17.2	15.8	19.7	18.0	19.4	18.2	21.4	20.1
18,000–33,333	32.8	28.7	29.1	33.4	33.4	33.3	29.9	37.1	33.3
Total flux in solar spectrum, W/m^2	995.4	1069.6	66.8	921.8	58.1	556.6	472.5	499.4	424.1
				$\theta_0 = 75°$					
0–1,000	0	0	0	0	0	0	0	0	0
1,000–2,500	0.4	0.2	0.3	0.1	0.2	0	0.2	0	0
2,500–4,400	1.3	1.5	1.5	0.7	0.9	0.2	0.9	0.1	0.6
4,400–6,200	5.0	5.5	6.6	4.1	5.1	2.4	4.9	2.0	3.8
6,200–8,200	6.3	9.3	10.9	5.7	7.0	6.6	9.3	4.0	5.9
8,200–9,700	6.1	7.9	9.2	5.9	7.3	7.9	8.8	5.9	6.9
9,700–11,500	8.1	9.8	11.2	8.0	9.6	10.4	10.9	8.3	9.3
11,500–13,000	9.2	8.2	9.1	9.0	10.2	8.9	9.0	9.4	9.8
13,000–14,500	8.5	8.1	8.9	8.4	9.5	8.8	8.8	8.8	9.2
14,500–18,000	20.2	17.1	18.3	19.8	21.4	19.0	18.3	21.0	20.8
18,000–33,333	35.0	32.4	24.0	38.2	28.7	35.9	29.1	40.5	33.7
Total flux in solar spectrum, W/m^2	279.6	207.0	108.2	175.2	90.5	88.3	211.0	78.3	182.0

Cloud optical depths τ of 1.0 and 9.7 and solar zenith angles (θ_0) of 30° and 75° (75.7° for the cloud-related cases) are considered. The total flux (W/m^2) in the 0–33,333 cm^{-1} regime is also listed. Surface albedo is assumed to be zero. Zeros in columns denote values <0.05%.

In examining the reasons for the accuracy of this technique, it is found that while there are several points at which the bin value of transmission can differ appreciably from the exact value (for the reasons mentioned earlier), both in the positive (>100%) as well as in the negative sense (up to ~100%), the sum over a large number of frequency points yields a small net difference. This is demonstrated by examining the maximum relative errors that occur when the bin results across the spectrum for $N = 90$ are grouped in frequency intervals of a specified width. The widths considered range from 1 cm^{-1} to a band (~1000 cm^{-1} or more) and eventually the total spectrum. The maximum relative errors are listed for the 180- to 200-, 580- to 600-, and the 800- to 820-mbar layers and for the two zenith angles in Table 7. The errors decrease with increasing size of the frequency interval for all cases. The bin results, when considered as sums over 500 cm^{-1} or more, are very accurate (better than 0.5%). It should be noted that the number of intervals with the maximum errors listed in Table 7 could be few or their absolute error could be small; in either case, the comparisons with exact values would be even more favorable.

The principal reasons for the accuracy of the binning method are the existence of a considerable number of frequency points and the presence of both positive and negative errors over a distribution of frequency points. In a sum over several wave number intervals (e.g., band), there occurs a substantial cancellation of the errors resulting in extremely precise solutions. These reasons are particularly important to remember when the number of bins used is small (say, $N = <9$) or when a small frequency interval (say, few wave numbers or individual frequency points) is being examined. Although the bin concept has been applied to all layers in this section, it is equally possible to apply it to a limited number of model layers.

The binning method affords only a marginal improvement over the exact method in terms of computational expense (Table 1), and hence there is little need to use the binning technique for the vapor-only benchmark computations. The virtue of the bin concept, however, is the substantial reduction made possible in the radiative transfer operations coupled with a negligible loss in the accuracy. This characteristic of the binning technique acquires considerably more significance when scatterers are considered in any layer, as will be seen in section 5.3.

At this stage, it is worthwhile recalling *Chou*'s [1986] inferences that there was no change in the heating rates when a spectral resolution of <0.5 cm^{-1} (down to 0.01 cm^{-1}) was used in a calculation framework involving equally spaced frequency points. Although the binning technique employs a different approach, the underlying reasons for the accuracy of the binning procedure could apply to Chou's monochromatic results as well.

It is important to note that the binning of optical depths is conceptually similar to the sorting of the absorption coeffi-

TABLE 5 Features of the Binning Procedure Adopted to Compute the Transfer of Radiation in an Inhomogeneous Atmosphere Containing Water Vapor

	First Bin in Decade		Last Bin in Decade		Maximum Relative
N	Range	Midpoint	Range	Midpoint	Error, %
900					0.5
90					5
9					50

N denotes the number of equally spaced intervals (or bins) per decade (p) in vapor optical depth, where $-12 < p < 2$. The range of the first and last bins (1.0^p) in each decade and the midpoints (1.0^p) of these intervals are listed. The maximum relative error that can be incurred due to binning in a homogenous layer is also listed for each N.

cients in the k-distribution method. In the latter technique, the sorting is performed at a reference pressure and temperature in conjunction with a scaling approximation [*Chou*, 1986]. This removes the dependence of the absorption coefficient on pressure and temperature, and the transmittance equation is reduced to an integration over the absorption coefficient. The binning method, in contrast, preserves the pressure and temperature dependences by considering the LBL-based values of the absorption coefficient at every monochromatic frequency in each layer; the approximation consists of merely an arbitrary degradation in the values of the absorption coefficients. The transfer equation, as in the LBL computations, is then solved for each frequency. These characteristics also distinguish the binning method from another approximation, the exponential-sum fitting technique [*Wiscombe and Evans*, 1977]. The latter method consists of a mathematical fit to a set of transmission values, in any spectral interval and for a range of scaled absorber path lengths, by a sum of exponentials. The individual terms represent pseudo-monochromatic transmittances which are then used to compute the transfer in the atmosphere. The derived terms, however, have no tangible links to the actual absorption lines (or to the LBL absorption coefficients) within the spectral interval.

4. Cloud Radiative Characteristics

In this section, the results of the 32-stream DA and DE calculations performed for the CL cloud (see ICRCCM specifications), and with no water vapor present (Figure 1*b*), are discussed. The cloud is assumed to be present in a 20-mbar-thick layer in order to compare with the vapor-only calculations of the preceding section. This is as if the solar irradiance at the top of the atmosphere were incident directly on the cloud. The frequency-dependent cloud single-scattering properties follow the ICRCCM tables (frequency notation is suppressed again); these are the extinction optical depth τ_{cld}, single-scattering albedo ω_{cld}, and asymmetry factor g_{cld}. The cloud-scattering optical depth is given by $\omega_{cld}\tau_{cld}$. Surface albedo is assumed to be zero throughout this section.

The band-by-band contribution to the heating rate for cloud optical depths of 1.0 and 9.7, respectively, are illustrated in Figure 9 (solid line). For either optical depth, solar zenith angles of 30° and 75.7° are considered. The contributions in the vapor-only case are also displayed for comparison. The relative contributions to the heating rate in the 800- to 820-mbar layer are tabulated in Table 3. Significant cloud particle absorption (>5%) occurs in nearly the same intervals (e.g., bands 3–5) as does the water vapor absorption. For the higher cloud optical depth, there is a dominant contribution from the 2500–8200 cm^{-1} spectral regions, while for the lower optical depth case, almost half the contribution arises from the 2500–4400 cm^{-1} interval alone. For the vapor-only case, contributions >5% occur in bands 3–9 (2500–14,500 cm^{-1}). For the cloud-only case, substantial increases occur in bands 2–5 compared to the vapor-only case. At $\nu > 11{,}500$ cm^{-1} (bands >7), the cloud drop absorption is quite small, whereas the vapor absorption

TABLE 6. Magnitudes of the Maximum Relative Errors in Atmospheric Heating Rates ($|\delta_{re}Q|$), Downward Flux at the Surface ($|\delta_{re}F_{sfc}|$), and Reflected Flux at the Top of the Atmosphere ($|\delta_{re}F_{TOA}|$)

	$\lvert\delta_{re}Q\rvert$ Maximum Error, %		$\lvert\delta_{re}F_{sfc}\rvert$ Maximum Error, %		$\lvert\delta_{re}F_{TOA}\rvert$ Maximum Error, %	
N	Band	Spectrum	Band	Spectrum	Band	Spectrum
			$\theta_0 = 30°$			
900	6.2×10^{-3}	2.1×10^{-3}	8.4×10^{-5}	3.0×10^{-5}	8.5×10^{-5}	4.0×10^{-5}
90	9.8×10^{-2}	3.8×10^{-2}	7.7×10^{-3}	2.4×10^{-3}	8.5×10^{-3}	3.0×10^{-3}
9	4.1×10^{-0}	1.9×10^{-0}	7.3×10^{-1}	2.2×10^{-1}	8.3×10^{-1}	2.7×10^{-1}
			$\theta_0 = 75°$			
900	6.3×10^{-3}	1.6×10^{-3}	1.0×10^{-4}	4.4×10^{-5}	1.6×10^{-4}	5.1×10^{-5}
90	9.9×10^{-2}	4.0×10^{-2}	9.1×10^{-3}	3.2×10^{-3}	1.1×10^{-2}	3.7×10^{-3}
9	4.2×10^{-0}	2.1×10^{-0}	9.0×10^{-1}	2.9×10^{-1}	1.0×10^{-0}	3.3×10^{-1}

Values are computed over bands and over the entire spectrum, obtained by comparing the binning method with the exact for the case of transmission of solar radiation through an inhomogeneous atmosphere containing only water vapor. Bin parameter N (see section 3.2) is assumed to be 900, 90, and 9, respectively, for solar zenith angles (θ_0) of 30° and 75°. Surface albedo is 0.2.

TABLE 7. Magnitude of the Maximum Relative Error (in Percent) in the Heating Rates Due Exact Results), for the Vapor-Only MLS Atmosphere

Width $\Delta\nu$, cm^{-1}	$\theta_0 = 30°$			$\theta_0 = 75°$		
	190 mbar	590 mbar	810 mbar	190 mbar	590 mbar	810 mbar
1	8.4×10^{1}	6.5×10^{2}	1.8×10^{3}	8.5×10^{1}	1.3×10^{5}	1.4×10^{6}
10	9.6×10^{0}	2.7×10^{1}	1.0×10^{2}	9.5×10^{0}	7.4×10^{1}	1.1×10^{3}
50	3.1×10^{-1}	6.4×10^{-1}	6.8×10^{0}	3.0×10^{-1}	3.9×10^{0}	3.1×10^{1}
100	2.3×10^{-1}	3.1×10^{-1}	6.8×10^{0}	2.3×10^{-1}	1.7×10^{0}	3.0×10^{1}
500	1.2×10^{-1}	3.0×10^{-1}	1.9×10^{-1}	1.1×10^{-1}	3.0×10^{-1}	1.9×10^{-1}
Band	5.2×10^{-2}	2.7×10^{-2}	4.0×10^{-2}	4.4×10^{-2}	2.2×10^{-2}	3.8×10^{-2}
Solar	9.0×10^{-3}	1.3×10^{-2}	1.0×10^{-2}	1.7×10^{-2}	1.2×10^{-2}	7.9×10^{-3}

The comparison is viewed in terms of sums over frequency intervals of uniform width $\Delta\nu$. Bin parameter N (see section 3.2) is 90 for solar zenith angles (θ_0) of 30° and 75°. Three layers, 180–200, 580–600, and 800–820 mbar, are examined. Widths of bands are listed in Table 2, while the width of the solar spectrum for heating rate purposes is 18,000 cm^{-1}.

extends all the way to 18,000 cm^{-1} (Figure 9). At the larger zenith angle, the contribution from the region beyond 11,500 cm^{-1} in the vapor-only case exceeds 15%.

The flux at the surface arises principally (contributions >3%) from bands with $\nu > 4400$ cm^{-1} for both the vapor and cloud-only cases (Table 4). Bands 10 (weakly absorbing) and 11 (nonabsorbing) contribute substantially (>17%). The absorbing bands together contribute more than 65%, just as in

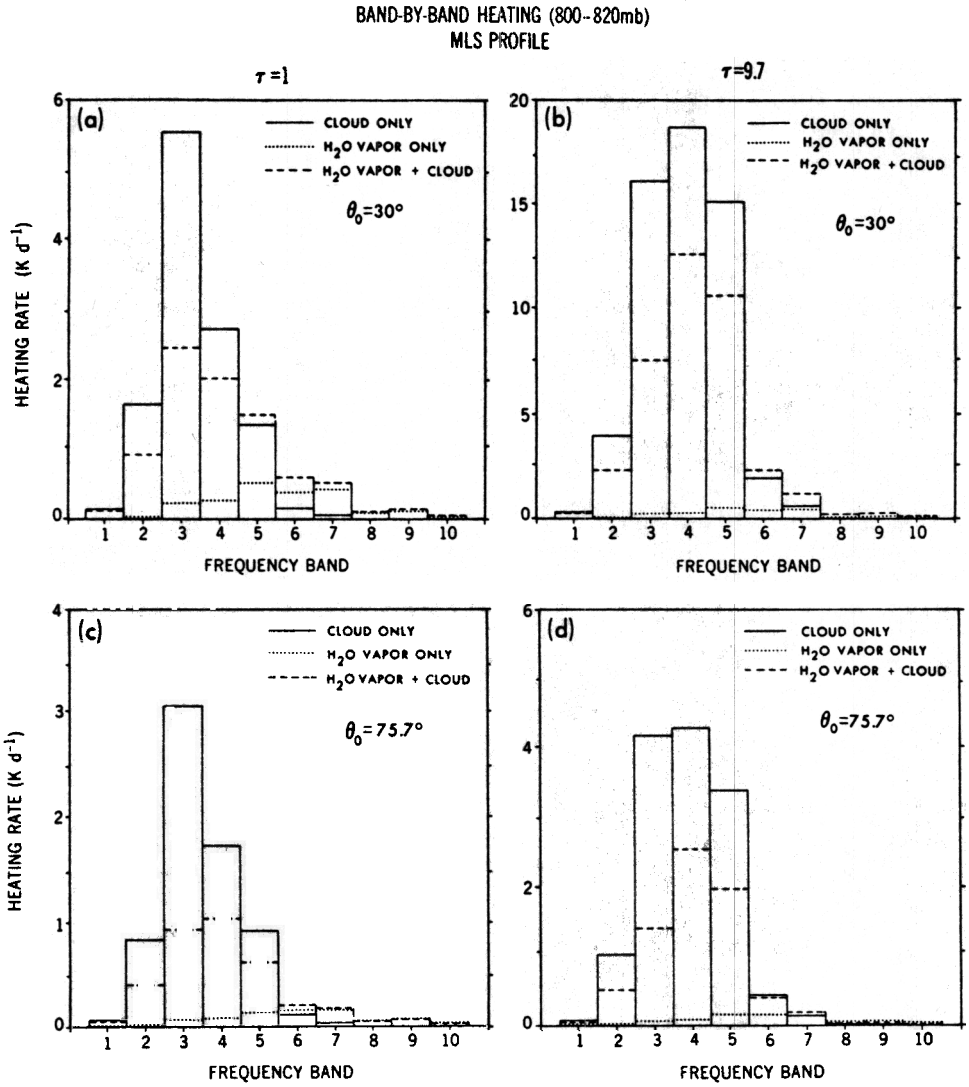

Fig. 9. Band-by-band contribution (0–18,000 cm^{-1}) to the heating rate in the 800- to 820-mbar layer of an MLS atmosphere for solar zenith angles θ_0 of 30° (upper panels) and 75.7° (lower panels). Three cases are considered in each panel: water vapor only, cloud only, and vapor plus cloud present in the atmosphere. The CL cloud is embedded in the concerned layer with an optical depth τ (λ=0.55 μm) of (*a* and *c*) 1 and (*b* and *d*) 9.7, respectively.

TABLE 8. Relative Error in the Downward Flux at the Surface ($\delta_{re}F_{sfc}$), the Reflected Flux at the Top of the Atmosphere ($\delta_{re}F_{TOA}$), and the Cloud Layer Heating Rate ($\delta_{re}Q$)

		0–18,000 cm^{-1}		18,000–33,333 cm^{-1}	
	θ_0, deg	$\delta_{re}F_{sfc}$, %	$\delta_{re}Q$, %	$\delta_{re}F_{sfc}$, %	$\delta_{re}F_{TOA}$, %
1.0	30	−0.5	−3.9	−0.6	11.4
1.0	75.7	11.7	−4.7	11.7	−21.3
9.7	30	1.7	−3.3	1.3	−1.7
9.7	75.7	11.3	2.2	11.5	−5.1
1.0	30	−0.6	−5.1	−0.6	11.3
1.0	75.7	11.0	−6.5	11.7	−21.3
9.7	30	0.8	−4.0	1.3	−1.7
9.7	75.7	10.6	2.5	11.5	−5.1

Values were obtained by comparing the results from the DE method with those from the DA (exact) method for a CL cloud in the 800- to 820-mbar layer of an MLS atmosphere containing no other component (cloud-only case; section 4) and with vapor (vapor-plus-cloud case; section 5.2), respectively. The frequency regions considered are 0–18,000 cm^{-1} and 18,000–33,333 cm^{-1}. The CL cloud has an optical depth τ of 1.0 and 9.7 at a wavelength of 0.55 μm; for each optical depth, solar incidence (θ_0) at 30° and 75.7° is considered.

the vapor-only case. When $\theta_0 = 30°$ and $\tau = 1$, there is more flux reaching the surface than in the vapor-only case; when $\tau = 9.7$, there is less flux reaching the surface than in the vapor-only case. When $\theta_0 = 75°$, both cloud types have less flux reaching the surface than in the vapor-only case. The examples studied here indicate that moderately thick clouds ($1 < \tau < 9.7$) in the atmosphere have a significant impact on the surface solar flux when compared to the effect due to the entire column of water vapor. Thus both vapor and droplet effects are equally important for the solar radiative interactions. The band-by-band relative contribution to the reflected flux exhibits features similar to those for the surface flux, with the sum from the absorbing regions exceeding 70%. For both transmission and reflection, these features are a consequence of a larger single-scattering albedo and a greater solar incident flux at the higher frequencies (Figure 2).

The comparisons of the errors due to the DE method in each band (not shown here) for the cloud-only case indicate that significant errors can arise in some bands. This is an important factor to be remembered, since the results for the entire spectrum suggest that the DE method is a good approximation, as seen by the relative errors listed in Table 8. The DE layer heating rates are within 5% of the exact values for all four cases; relative errors in fluxes can reach 10% or more (e.g., surface flux for $\theta_0 = 75.7°$; reflected flux for $\tau = 1$). For $\tau = 1$ ($\theta_0 = 75.7°$), both reflected and surface fluxes are poorly represented (errors >10%) by the DE approximation. In the 18,000–33,333 cm^{-1} interval, there is negligible absorption by pure drops, and so absolute errors in reflected and transmitted fluxes take on equal and opposite signs. Again, the relative errors for the $\theta_0 = 75.7°$, $\tau = 1$ case are the worst among those studied here; this is consistent with the tests of *King and Harshvardhan* [1986].

The vertical profile of the total heating rate for the cloud-only case ($\tau = 1$) is shown in Figure 10 and, for comparison, the vapor-only results are also shown; the zenith angles are 30° and 75°, respectively. Even for a cloud optical depth of 1.0, there is substantial enhancement in the solar heating of the 800- to 820-mbar layer compared to the vapor-induced heating. For $\tau = 9.7$, the enhancements with respect to vapor are more than for the case when $\tau = 1$ (see Table 3). The ratio of the enhancement at $\tau = 9.7$ to that at $\tau = 1$ is 4.9 (2.0) for a 30° (75.7°) solar incidence.

5. Water Vapor Absorption and Cloud Extinction

In this section, the radiative transfer due to the CL cloud embedded in an MLS atmospheric profile is studied (Figure 1*c*). As in section 4, the cloud is assumed to be located in the 800- to 820-mbar layer. The frequency-dependent cloud single-scattering properties follow the ICRCCM specifications for the CL cloud. Solar zenith angles of 30° and 75.7° and the cloud optical depths of 1.0 and 9.7 are considered in an MLS atmosphere. Surface albedo is again assumed to be zero.

The presence of water vapor introduces an important modification to the single-scattering properties of the layer containing the cloud [*Twomey*, 1976]. The vapor absorption optical depth, since it arises due to the vibrational-rotational structure and is necessarily finely spaced in frequency, exhibits a sharp variation across the spectrum. For a layer containing the cloud, the presence of vapor renders a correspondingly fine structure in the layer radiative properties. While a calculation for the cloud-only case can be met with a coarse resolution calculation involving only 107 intervals (as in section 4), a finer spectral resolution is required when the vapor too has to be considered. The resolution to be employed for a precise computation is dictated by the LBL features of the vapor molecule and thus must be similar to that employed for the exact computations in section 3.

The total optical depth in the multiple-scattering algorithms for the layer at any frequency point i (in a wave number interval) is now given by

$$\tau_{tot,i} = \tau_{cld} + \tau_i \tag{10}$$

while the corresponding layer single-scattering albedo becomes

$$\omega_i = \omega_{cld}\tau_{cld}/\tau_{tot,i} \tag{11}$$

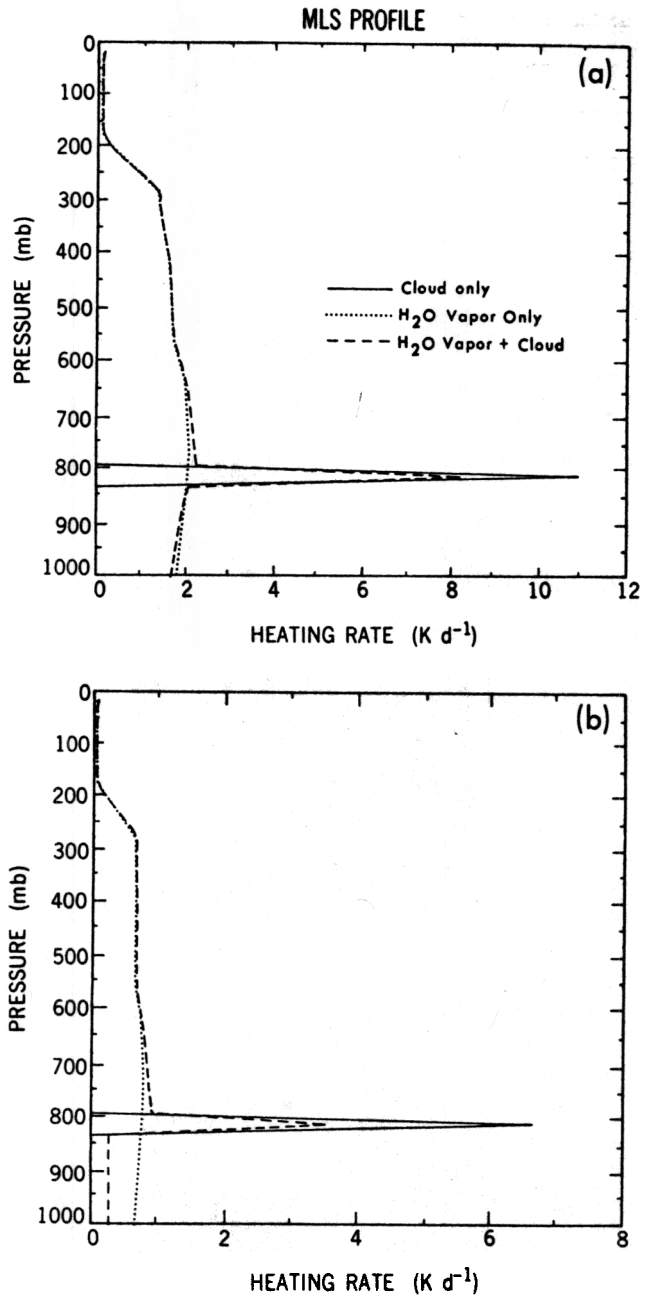

Fig. 10. Vertical heating rate profile in the MLS atmosphere for solar zenith angles θ_0 of (*a*) 30° and (*b*) 75.7°. The three cases are the same as in Figure 9; cloud optical depth $\tau = 1$. There is a sharp increase in the heating at 810 mbar due to the cloud.

The scattering optical depth at any frequency and in the cloud layer has the same value as for the cloud-only case in the previous section ($\omega_{cld}\tau_{cld}$); however, the layer absorption optical depth varies at each frequency point i in any wave number interval, resulting in a corresponding variation of the layer extinction and the layer single-scattering albedo. For all frequency points in a 1 cm^{-1} interval, the cloud properties are assumed constant. Consideration of the molecular absorption, however, introduces a weight factor (w_i) to the transfer at the ith frequency point.

Compared to the cloud-only case, in the case of a typical atmospheric profile, i.e., water vapor present as an inhomogeneously distributed absorber, there is a differential attenuation of the direct beam at the different frequency points before it is incident at the cloud top. Thus the incident irradiance and its spectral distribution will be different at the cloud top (800 mbar) from that at the top of the atmosphere; the lower the altitude of the cloud location, the more the difference relative to the irradiance distribution outside the atmosphere.

We discuss below the results using three different techniques to solve for the radiative transfer in the inhomogeneous atmosphere containing cloud and water vapor. The techniques for computing the vapor-cloud interactions are designated, for ease of reference, by the letters VC. The first technique discussed (VC1) represents the most precise calculation of the radiative transfer performed in this study. Results from the other techniques are compared with the VC1 solutions in the subsequent subsections.

5.1. *VC1 (Exact) Technique*

The most precise technique combines the LBL algorithm (sections 2.1, 3.1) with the 32-stream, DA method (section 2.2). At each of the 2.8×10^6 frequencies, the solutions are obtained for the reflected (R) and transmitted (T) radiance matrices in each of the 32 directions (or streams) for the scattering-absorbing layer.

The direct beam interaction with water vapor above the cloud layer is performed in the same manner as in the vapor-only case (equations (1) and (2)). Given an incident beam at the cloud top, the R and T matrices [*Coakley et al.*, 1983] are obtained for the cloud layer at each frequency point i within a wave number interval. These provide boundary conditions for the upward radiances ($I_{i,k}^{\uparrow}$) leaving the cloud top (level LT) and for the transmitted radiances ($I_{i,k}^{\downarrow}$) leaving the cloud base (level LB), where μ_k is the cosine of the zenith angle of an emergent stream k from the cloud,

$$I_{i,k}^{\uparrow} = \mu_k R_{i,k} \quad \text{at LT} \tag{12}$$

$$I_{i,k}^{\downarrow} = \mu_k T_{i,k} \quad \text{at LB} \tag{13}$$

Next, transmission matrices in the k direction for each of the water vapor layers above and below the cloud are obtained (equation (1) with μ_k replacing μ_0), thus yielding the upward radiances above the cloud top (say, level L1) and the downward radiances below the cloud base (say, level L2)

$$I_{i,k}^{\uparrow} = \mu_k R_{i,k} \prod_{l=\text{L1}}^{\text{LT}-1} [\exp(-\tau_{i,l}/\mu_k)] \quad \text{at L1} \tag{14}$$

$$I_{i,k}^{\downarrow} = \mu_k T_{i,k} \prod_{l=\text{LB}}^{\text{L2}-1} [\exp(-\tau_{i,l}/\mu_k)] \quad \text{at L2} \tag{15}$$

An angular integration of the radiances yields the corresponding up and down fluxes at the concerned frequency:

$$F_{i,\text{L1}}^{\uparrow} = \sum_{k=1}^{32} I_{i,k}^{\uparrow} w_k^*$$

$$F_{i,\text{L2}}^{\downarrow} = \sum_{k=1}^{32} I_{i,k}^{\downarrow} w_k^*$$

where w_k^* is the weight of a particular stream to the flux and depends on the quadrature scheme.

The net flux at all levels above the cloud consists of the downward (direct) flux (equation (2)) and the upward diffuse (reflected) flux (equation 16)). The net flux at levels below the cloud, under the assumption of a zero surface albedo, is merely the downward transmitted flux (equation (17)). After the fluxes have been obtained at each of the frequencies within a wave number interval, the weight factors w_i (contribution from the ith frequency point) are employed to obtain the fluxes in the wave number interval (equation (7)). The layer heating rates are evaluated as in section 3.1 (equations (6) and (9)).

A measure of how sharply the absorption in the cloud layer varies as a function of frequency can be had from the limited interval results presented in the appendix (Figure A3c). The rest of this subsection concerns the fluxes and heating rates in the different bands across the solar spectrum. Before discussing the specifics, it is important to state that the relative spectral effects of water vapor and water drops obtained here are qualitatively similar to the narrow-band model results [*Davies et al.*, 1984; *Wiscombe et al.*, 1984].

The exact vapor-plus-cloud results (VC1) for the band-by-band contribution to the heating in the 800- to 820-mbar layer are compared with the corresponding cloud-only and the vapor-only results in Figure 9 (dashed line) (see Table 3 for the relative contributions). The contribution from each band is, in general, a superposition of the vapor and cloud absorption effects discussed in sections 3 and 4, respectively, with the cloud effects being accentuated for the larger optical depth case.

There is significant enhancement with respect to vapor contributions even for $\tau = 1$, just as in the cloud-only case (see also *Wiscombe et al.* [1984]). Bands 2–7 are the most important contributors; bands 2 and 3 may seem surprising, since there is very little incident irradiance in these intervals (Figure 2). This, however, is more than compensated for by the strong cloud absorption at these intervals.

Compared to the cloud-only case, water vapor in the present case exercises two distinct effects [*Davies et al.*, 1984]: (1) it depletes the beam incident on the cloud, particularly for those bands which absorb strongly at altitudes above the cloud top, and (2) it contributes additional absorption in the cloud layer. The comparison of the magnitudes for the cloud-only and the vapor-plus-cloud cases in any band represents a combination of the two opposing tendencies. The manifestation of the effects introduced by the vapor depends on the cloud optical properties. In particular, the effect of water vapor absorption in any band is small if the cloud optical depth is large.

The 2500–4400 cm^{-1} region (band 3), which exhibited a strong absorption for the cloud-only case, has diminished in importance (Figure 9), owing to strong vapor absorption above the cloud layer. For $\tau = 1$ the absolute contributions show that the vapor-plus-cloud heating exceeds that in the cloud-only case ($\theta_0 = 30°$) for bands >4; at $\theta_0 = 75.7°$, the vapor-plus-cloud heating exceeds that due to cloud alone for bands >5. This is due to water vapor absorption in the cloudy layer. For $\tau = 9.7$, this feature occurs for bands >5 ($\theta_0 = 30°$) and 6 ($\theta_0 = 75.7°$), respectively. This shift in band number for the higher zenith angle, in order for the above-mentioned transition to occur, is due to the longer path lengths at 75.7°; this causes the heating due to water vapor in the 800- to 820-mbar layer to diminish in any band, when compared to the 30° incidence (Figure 7). Thus at 75.7°, only the higher numbered bands, which contain a greater solar irradiance and suffer less attenuation in the atmosphere will be of significance for the additional heating due to water vapor in the 800- to 820-mbar layer. Water vapor absorption contributes more than droplet absorption in bands ≥8; the absolute magnitudes, however, in these intervals, contribute very little to the total heating (Figures 5 and 6).

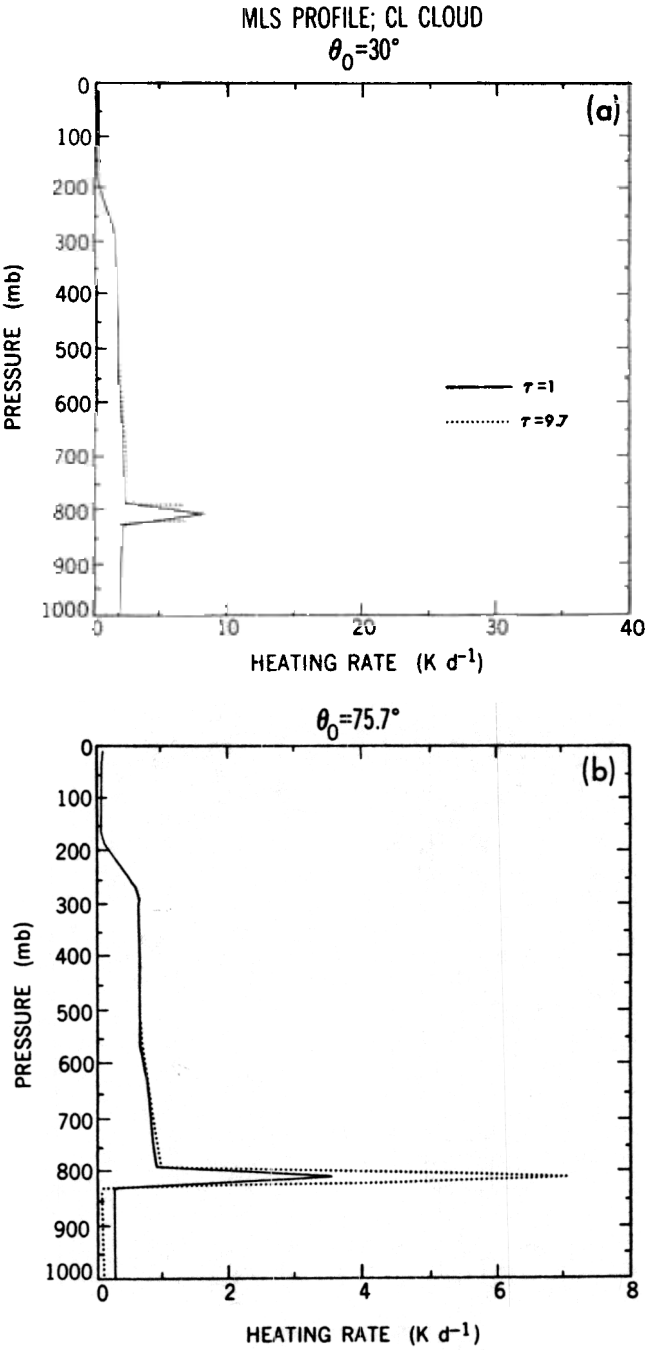

Fig. 11. Vertical heating rate profile for the case of an MLS atmosphere containing water vapor and CL cloud embedded in the 800- to 820-mbar layer. Cloud optical depth τ is 1 and 9.7, respectively. Solar zenith angle θ_0 is (*a*) 30° and (*b*) 75.7°. Note the increase in the heating at 810 mbar caused by an increase in τ.

For $\tau = 9.7$ the cloud effects dominate over that of vapor in the layer, so that there is a much stronger resemblance to the results from the cloud-only case, although the vapor attenuation of the direct beam above the cloud reduces the magnitude of heating in any band (<6) for both zenith angles. The fact that cloud effects for $\tau = 9.7$ dominate over that for vapor in the heating of the 800- to 820-mbar layer becomes evident on comparing the vapor only and vapor-plus-cloud results in Table 3.

The vertical profiles of the total heating for $\tau = 1$ and for the two zenith angles are shown in Figure 10; the results are compared with those from the vapor-only and the cloud-only cases. The enhancement in the 800- to 820-mbar layer heating due to water drop absorption (over the vapor only case) is prominent again, but there is also a decrease below the cloud; this represents a reduction below the values for the vapor-only case (12% for $\theta_0 = 30°$ and 50% for $\theta_0 = 75.7°$ at ~1000 mbar). Above the cloud, there is little change from the vapor-only case, owing to the heating there resulting mainly from the direct beam absorption. The reflected beam from the cloud top causes a small addition to the heating in the layers just above the cloud.

Figure 11 illustrates the large heating rates that occur in cloudy layers due to increases in extinction optical depths. For $\tau = 9.7$ the increase in the 800- to 820-mbar layer heating is 4.5 ($\theta_0 = 30°$) and 2.0 ($\theta_0 = 75°$) times, respectively, that for $\tau = 1$. The increase is nearly independent of the vapor attenuation of the direct beam above the cloud, so that the ratios at the two zenith angles are almost similar to the corresponding results from the cloud-only case (section 4).

The band-by-band contributions to the vertical heating rate profile for the $\tau = 1$ case are displayed in Figures 12 and 13 for zenith angles of 30° and 75.7°, respectively. These may be directly compared with the corresponding figures 5 and 6 for the vapor-only case. The bands responsible for the heating in the cloudy layer (2–7, discussed earlier in the context of Figure 9) are apparent from the peaks in the curves at $P = 810$ mbar. Below the cloud, bands below 8200 cm^{-1} exhibit a decrease in the heating rate when compared to the vapor-only case. This is true for both zenith angles. For bands above 8200 cm^{-1}, too, there is a decrease. In fact, for $\theta_0 = 30°$ the depletion of the irradiance in the 8200–11,500 cm^{-1} interval below the cloud indicates a partial saturation effect occurring in the 800- to 820-mbar layer; in contrast, the vapor-only case (Figure 5) does not exhibit such an effect in that interval. For $\theta_0 = 75.7°$ (Figure 13) the apparent saturation effect induced by the cloud layer extends to all bands; the corresponding vapor-only case (Figure 6) exhibits such an effect only for bands below 11,500 cm^{-1}.

The band-by-band contributions to the downward flux at the surface and the upward flux at the top of the atmosphere are listed for all cases in Table 4. Bands 5–9 (6200–14,500 cm^{-1}) contribute ~4% or more, while bands 10 and 11 (14,500–33,333 cm^{-1}), just as in the vapor-only and cloud-only cases, are dominant contributors. As noted earlier, this is due to the solar irradiance distribution (Figure 2) and the increase in cloud single-scattering albedo with frequency.

Comparing with the cloud-only situation, while the total flux is less, the relative contribution from the nonabsorbing band (band 11) increases for both the surface and the top of the atmosphere reflected fluxes; the sum from the absorbing regimes (bands 1–10) decreases. Comparison of the surface flux with the vapor-only situation reveals the same features.

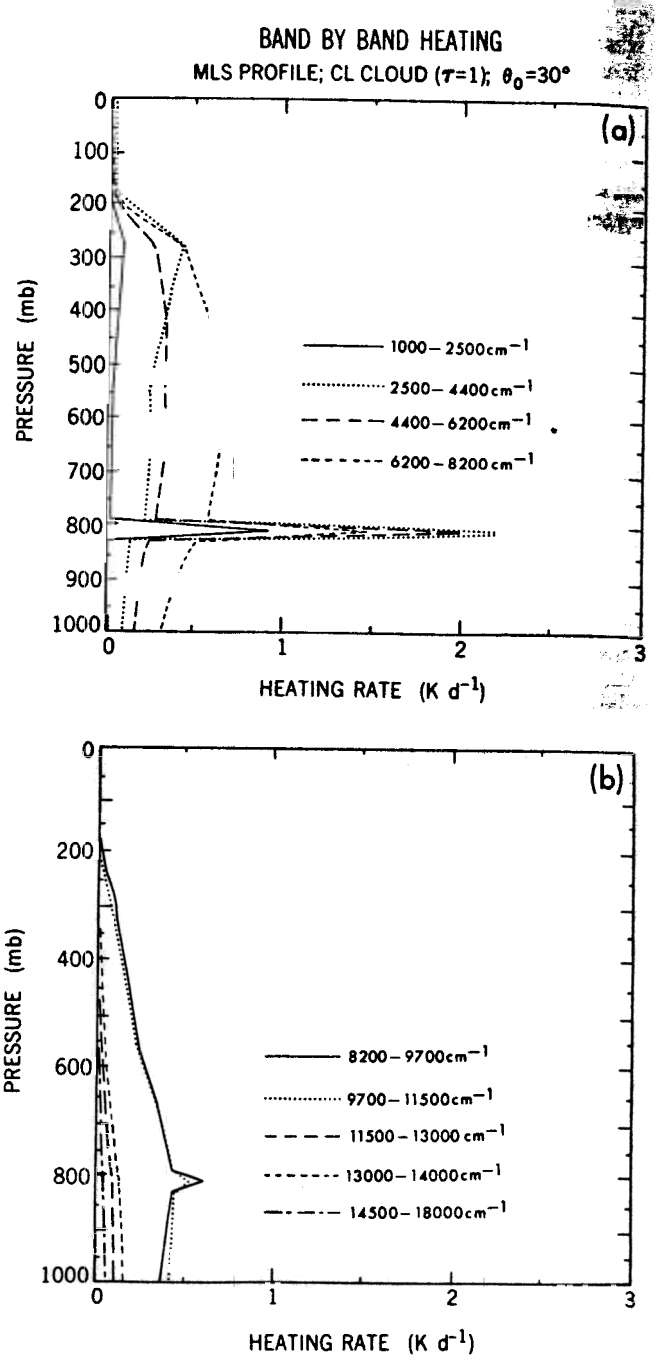

Fig. 12. Same as Figure 5, except in the case of a CL cloud of optical depth $\tau = 1$ located in the 800- to 820-mbar layer of an MLS atmosphere. The peaks in the curves at 810 mbar are due to the cloud properties in the respective bands.

For any of the situations shown in Figure 1, bands 2–9 contribute more than band 10 to the fluxes at the atmospheric boundaries; further, the 0–18,000 cm^{-1} contribution exceeds that from the 18,000–33,333 cm^{-1} interval.

In all but one of the cases listed in Table 4, the surface flux decreases in going from vapor-only to cloud-only to vapor-plus-cloud situation. The exception is the $\tau = 1$ (30°) case which has the largest value for the cloud-only situation. The sensitivity of the 0–18,000 cm^{-1} fluxes to the spectral features of vapor, droplet properties, and zenith angle em-

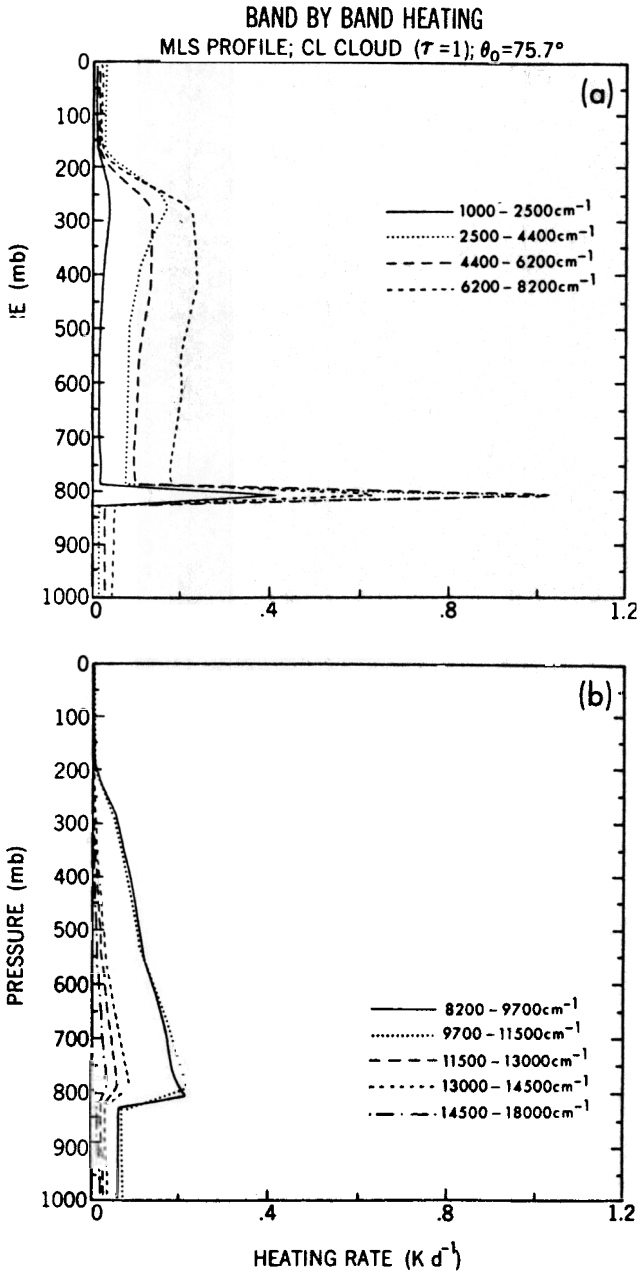

Fig. 13. Same as Figure 6, except in the case of a CL cloud of optical depth τ = 1 located in the 800- to 820-mbar layer of an MLS atmosphere (zenith angle θ_0 = 75.7°). The peaks in the curves at 810 mbar are due to the cloud properties in the respective bands.

phasizes the necessity of high-resolution computations to determine cloud radiative interactions accurately.

5.2. *VC2 Technique*

It has been possible to investigate only a few cases for the entire spectrum using the LBL + DA method because of the computational expense involved (Table 1). One of the more economical ways to solve the radiation problem is to approximate the scattering processes by a suitable two-stream method, while maintaining the line-by-line structure of the transfer algorithm. Here we pursue the DE approximation; the LBL + DE method is designated as the VC2 technique.

The treatment of cloud extinction by the DA or DE method, besides introducing a different approach in the computation of the cloud layer radiative properties, also introduces a difference in the computation of the net fluxes in the layers above and below the cloud. The DA method treats multiple streams of radiation and, for both the reflected and transmitted beams leaving the cloud, the angular dependences are explicit in the computation of the fluxes at each level. The DE approach, in contrast, simplifies the computational problem (see *Joseph et al.* [1976] for the cloud reflectivity and transmissivity equations) of the attenuation of the reflected and transmitted beams leaving the cloud top and cloud base. The reflected beam is diffuse, and its propagation is described by an equation similar to (4), with the cloud top replacing the surface as the lower boundary. The transmitted beam consists of both the direct (T) and the diffuse (T^*) beams and is described by an equation similar to (2). As in section 5.1, the net flux above the cloud consists of the downward (direct) beam and the upward diffuse (reflected) beam, while the net flux below the cloud consists of only the transmitted beam. The fluxes and heating rates over 1 cm^{-1} or larger intervals are obtained as before.

The effects of water vapor on the radiative properties of a cloudy layer and the differences introduced by the DE approximation are discussed in the appendix. Depending on the vapor optical depth, substantial departures from the exact results can occur at discrete frequencies due to the DE approximation. Further, relative errors for the sums over any interval (say, 5 cm^{-1}) in the cloudy layer of an inhomogeneous atmosphere follow approximately the errors predicted by a homogeneous layer computation that considers an identical range of vapor optical depth values occurring in that interval.

We compare the results from the VC2 technique with those from the VC1 technique for the entire spectrum below.

The vertical profile of the relative error in heating for the VC2 results is shown in Figures 14*a* and 14*b* for the two cloud optical depths and the two solar zenith angles, respectively. There is an underestimate of cloud layer heating in all the cases, except at τ = 9.7 (75.7° incidence). For 30° there is an overestimate both above and below the cloud at τ = 9.7. For 75.7°, there is still an overestimate below but an underestimate above at both τ. The relative errors are largest in the layers directly beneath the cloudy layer (up to 32% at τ = 9.7).

The magnitude of the relative error in heating ($|\delta_{re}Q|$) for each band in the 800- to 820-mbar layer (both optical depths and both zenith angles) is illustrated in Figure 15. Errors for τ = 1 attain large values (up to 16%) at the higher frequency bands. Considering the first nine bands, errors are <13%. The large error in band 10 is not significant for the error in total heating owing to its small absolute value (Figures 12 and 13). For τ = 9.7 the results are in better agreement with the VC1 results; again, band 10 has the largest relative error, while the rest of the bands have errors of <10%.

The solar heating rate errors for the cloud layer from the VC2 method are within 7% for both zenith angles (Table 8) and are slightly worse than in the corresponding cloud-only case. Since most of the heating in the layers well above the cloud (P < 600 mbar) is due to direct beam absorption, there is little difference (<2%) there between the VC1 and the VC2 methods (Figure 14).

The magnitudes of the relative error in the fluxes at the

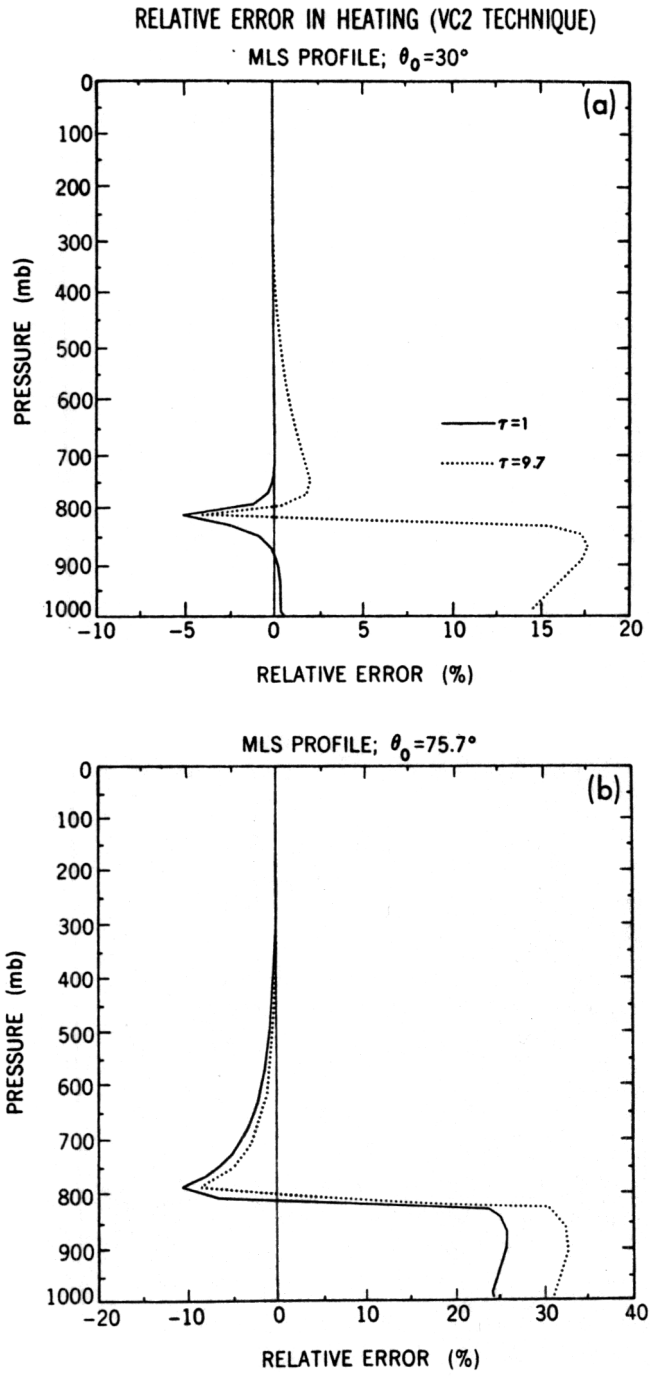

Fig. 14. Vertical profile of the relative error in the heating rate, as obtained by comparing the VC2 method results with the VC1 (exact) results for a CL cloud of optical depth τ = 1 and 9.7, respectively, located in the 800- to 820-mbar layer of an MLS atmosphere containing water vapor. Solar zenith angle θ_0 is (*a*) 30° and (*b*) 75.7°.

surface ($|\delta_{re}F_{sfc}|$) and at the top of the atmosphere ($|\delta_{re}F_{TOA}|$) in each band are illustrated in Figure 16 for the two optical depths and for the two zenith angles. At the surface (Figure 16, lower panels) the errors are <12%, except in bands 1 and 2 (0–2500 cm^{-1}) for τ = 9.7 (θ_0 = 30°); these bands, however, contribute little to the total flux (Table 4). At the top of the atmosphere (Figure 16, upper panels), errors can exceed 10% in all the bands for τ = 1. For τ = 9.7, errors are <10%, except in bands that contribute negligibly.

The relative errors in the total flux for both the water vapor absorbing spectral intervals (0–18,000 cm^{-1}) and the rest of the spectrum (18,000–33,333 cm^{-1}) are listed in Table 8. The flux at the surface differs by up to 12% between the two methods for the 75.7° incidence; smaller (<2%) relative errors occur for the 30° incidence. The reflected flux at the top of the atmosphere is in error by ~20% (τ = 1); smaller errors (~5%) occur for τ = 9.7.

The above results suggest that, even for the limited number of cases examined here (with respect to zenith angle and/or cloud optical depth), it is not possible to regard the LBL + DE (VC2) technique as a substitute for the exact method. It does, however, yield a reasonable first-order approximation of the spectrally integrated quantities. Owing to its efficiency (CPU time ~0.5 hours; Table 1), it is useful for gaining insights into the distribution of fluxes and heating rates for various types of cloudy atmospheres.

5.3. *VC3 Technique*

The computational burden of the VC1 technique can be reduced by decreasing the number of frequency points at which the radiative transfer equation is being solved. This can be accomplished by employing the bin concept described in section 3.2 and the binning method can be associated with the DA algorithm. This technique also involves the LBL features of the vapor and is designated here as VC3. Again, the binning is performed with respect to the vapor optical depth. There are, however, some differences between the way the binning concept is applied here and the manner in which it was applied to the vapor-only case.

The DA algorithm in the present technique considers the total optical depth at any frequency as the sum of the cloud extinction optical depth and the bin value of the vapor optical depth. For a given set of cloud single-scattering properties, the binning is performed over the range of vapor optical depth values in the model atmosphere. Equations (10) and (11) are modified in the VC3 technique by replacing the value of τ by τ', just as in section 3.2. Thus the equations for the total layer optical depth and the layer single-scattering albedo become for a frequency point in a 1 cm^{-1} interval

$$\tau'_{tot,i} = \tau_{cld} + \tau'_{v,i} \tag{18}$$

and

$$\omega'_i = \omega_{cld}\tau_{cld}/\tau'_{tot,i} \tag{19}$$

The scattering optical depth and the phase function at each frequency remain the same as for the VC1 technique.

Section 3.2, in contrast to the present application, considered the bin value of the vapor optical depth to be the only entity needed for the calculation of the radiative (viz., transmission) properties of the entire atmosphere. In the present vapor-plus-cloud case, layers not containing the cloud undergo an exact calculation, as in section 5.1; only the cloud layer undergoes the binning process. At each frequency point, just as in the vapor-only case, radiative properties (i.e., reflection and transmission matrices for the primed quantities) corresponding to the bin value of the vapor optical depth are computed for the cloudy layer. For the noncloudy layers above and below the cloud, only the

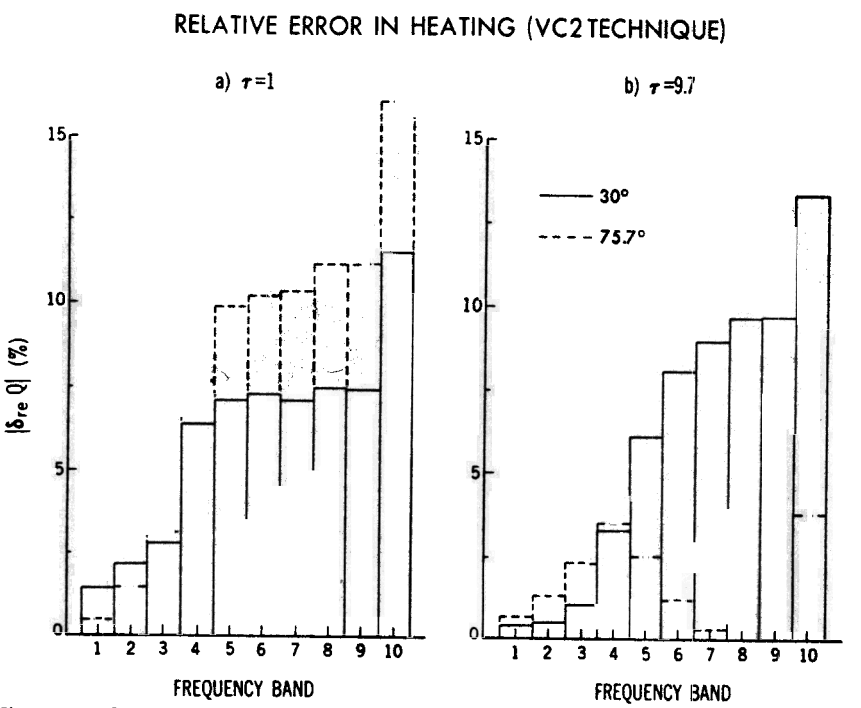

Fig. 15. Histogram of the relative errors in the 800- to 820-mbar layer heating rate ($|\delta_{re}Q|$%) for each band, as obtained by comparing the VC2 and the VC1 (exact) techniques. Cloud optical depth τ is (*a*) 1 and (*b*) 9.7 for zenith angles θ_0 of 30° and 75.7°.

transmission function need be computed for each of the 32 reflected and transmitted streams, respectively. The equations for the radiances and the procedure for the evaluation of the fluxes follow those described for the VC1 technique (see equations (12)–(17)).

For the present purpose, the lower limit chosen for the binning technique is 10^{-6} (the results are negligibly altered by a value less than 10^{-6}); the upper limit remains at 10^2. Again, a zeroth bin is designated, this time for all $\tau < 10^{-6}$. There is now variation of eight orders of magnitude in the vapor optical depth to be accounted for by the bins, so that the number of bins required to perform the transfer in the 0–18,000 cm^{-1} regime is $8N$.

The binning procedure is performed separately for each set of cloud single-scattering properties. There are 97 different wavelengths in the 0–18,000 cm^{-1} regime at which the cloud properties are tabulated, so that the binning process is undertaken 97 different times. Recall that in the vapor-only case (section 3.2), only one set of binning operations was necessary for the entire 0–18,000 cm^{-1} interval. For example, if N, the binning parameter (or number of points per decade in optical depth; see Table 5) is set at 90, the vapor-only case would require consideration of only ~720 different intervals (to account for 8 orders of magnitude variation in optical depth), whereas to do the vapor-plus-cloud problem would require, in general, 720 × 97 or ~70,000 different intervals. In comparison to the exact (VC1) calculation, however, there still results about a factor of 40 fewer calculations.

The accuracy of the binning method is investigated by considering first the magnitude of the maximum relative errors in the heating rates occurring anywhere in any band and across the spectrum. These are listed in Table 9 for N = 90 and 9 (the cloud optical depth is unity). The maximum band errors occur for the cloud layer. The relative errors for the 30° incidence are small in all bands (<0.6% for N = 90 and <4% for N = 9); maximum relative errors occur for bands (e.g., band 10) whose contributions to the total heating (Figure 12) are small. For the larger zenith angle, the errors tend to be even smaller. The relative errors in the total heating rate for both zenith angles anywhere are extremely small: <0.02% for N = 90 and <1.0% for N = 9. The vertical profile of the relative error in the total heating is illustrated in Figure 17 for N = 90 and 9 and indicates that peak errors occur in the cloud layer.

As in the vapor-only case, we inquire into the magnitudes of the relative error in the heating rate when the bin results for N = 90 are grouped in frequency intervals of specified widths. Table 10 lists, for each width chosen, the number of intervals (as a fraction of the total) with relative errors in three ranges: <0.1%, 0.1–1%, and ≥1%. The number of intervals with errors ≥1% decreases with increasing frequency width (i.e., increasing number of frequency points); for a $\Delta\nu$ of 500 cm^{-1}, only 6% (or two) of the intervals have ≥1% error, while band and spectrum results are below 1% in error. Errors for a cloud optical depth of 9.7 (not shown here) are smaller than those for 1.0.

The relative error in the fluxes at the top of the atmosphere and that at the surface for each band are listed in Table 9. The errors for N = 9 are less than 0.06% for both zenith angles and with respect to both sets of fluxes. The N = 90 case exhibits even smaller errors.

The above results demonstrate that the bin method is capable of yielding extremely accurate results at a considerably (~25 times) less computational expense (Table 1) than the exact (VC1) technique. The discussions given for the binning technique in the case of the vapor-only atmosphere (section 3.2) hold true even here. Although large relative errors can result at any specific frequency, the summation over bands, together with a judicious selection of the bin resolution can provide extremely accurate benchmark re-

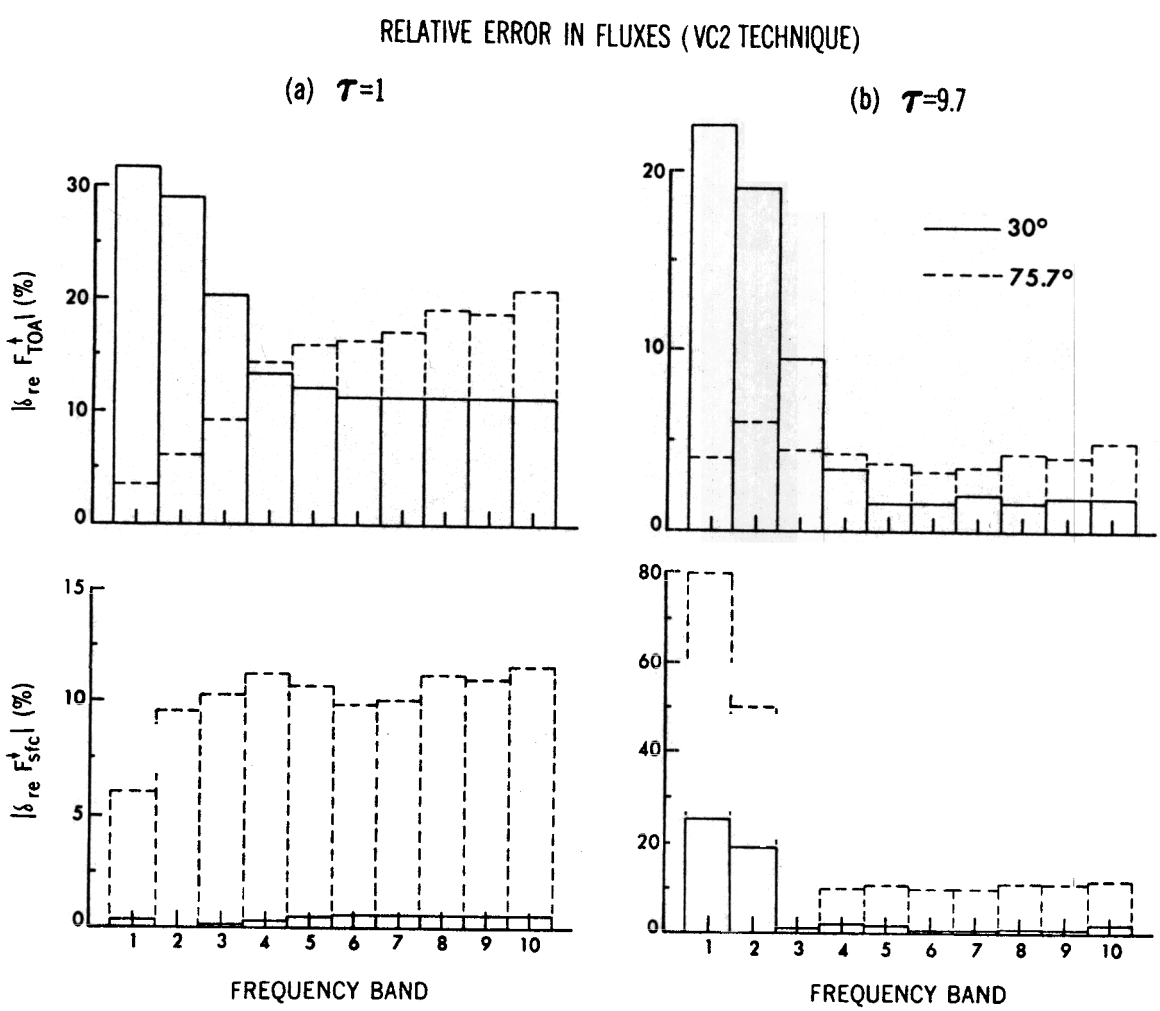

Fig. 16. Histogram of the relative errors in the reflected flux at the top of the atmosphere ($|\delta_{re}F_{TOA}|$%) (upper panels) and the downward flux at the surface ($|\delta_{re}F_{sfc}|$%) (lower panels) for each band, as obtained by comparing the VC2 and VC1 (exact) techniques. Cloud optical depth τ is (*a*) 1 and (*b*) 9.7 for zenith angles θ_0 of 30° and 75.7°.

sults for the fluxes and heating rates in cloudy inhomogeneous atmospheres. This is very encouraging inasmuch as it becomes possible to substitute this method for the computationally burdensome VC1 in future benchmark calculations.

6. Conclusions

A major new initiative has been undertaken at the Geophysical Fluid Dynamics Laboratory (GFDL) to prepare

TABLE 9. Magnitudes of the Maximum Relative Errors in the Atmospheric Heating Rates ($|\delta_{re}Q|$), the Downward Flux at the Surface ($|\delta_{re}F_{sfc}|$), and the Reflected Flux at the Top of the Atmosphere ($|\delta_{re}F_{TOA}|$)

	$\lvert\delta_{re}Q\rvert$ Maximum Error, %		$\lvert\delta_{re}F_{sfc}\rvert$ Maximum Error, %		$\lvert\delta_{re}F_{TOA}\rvert$ Maximum Error, %	
N	Band	Spectrum	Band	Spectrum	Band	Spectrum
			$\theta_0 = 30°$			
90	5.3×10^{-1}	1.6×10^{-2}	7.4×10^{-3}	2.6×10^{-4}	2.4×10^{-2}	6.4×10^{-4}
9	3.5×10^{-0}	8.6×10^{-1}	3.1×10^{-2}	9.1×10^{-3}	5.6×10^{-2}	2.0×10^{-2}
			$\theta_0 = 75.7°$			
90	2.2×10^{-1}	1.0×10^{-2}	1.9×10^{-2}	3.6×10^{-4}	2.1×10^{-2}	4.3×10^{-3}
9	3.1×10^{-0}	4.3×10^{-1}	3.0×10^{-2}	1.2×10^{-2}	3.4×10^{-2}	1.5×10^{-2}

Values were computed over any band and over the entire spectrum, obtained by comparing the binning method with the exact for the vapor-plus-cloud (optical depth = 1) case (section 5.3). Bin parameter N is assumed to be 90 and 9, for solar zenith angles (θ_0) of 30° and 75.7°.

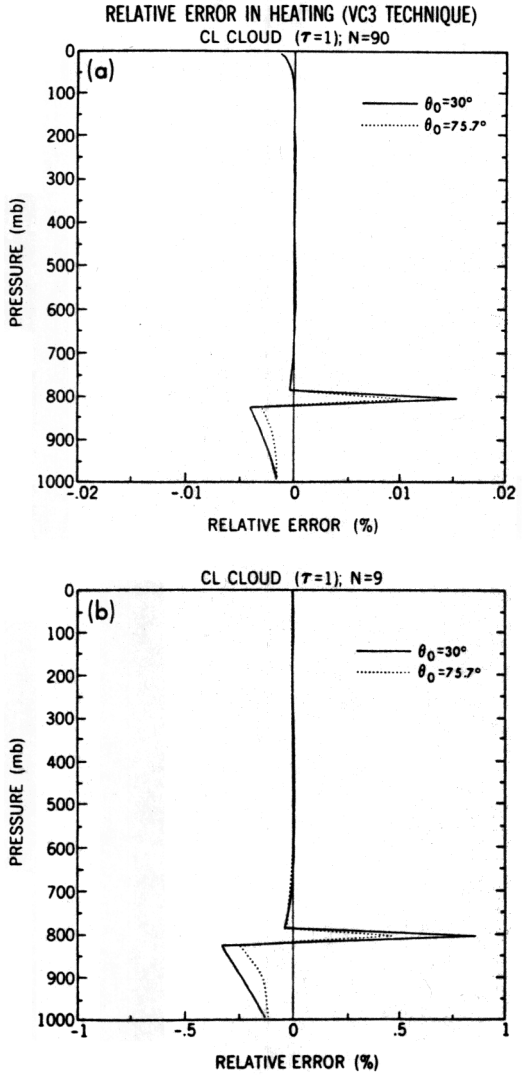

Fig. 17. Vertical profile of the relative error in the total heating rate, as obtained by comparing the results from the VC3 (bin) and the VC1 (exact) techniques. Bin parameter N is (*a*) 90 and (*b*) 9. Solar zenith angles θ_0 of 30° and 75.7° are considered for cloud optical depth τ of 1.

benchmark solutions for the solar radiative transfer in scattering-absorbing atmospheres containing water vapor and plane-parallel clouds with specific optical properties. Considerations of the very fine structure of the spectral absorption of the water vapor molecule and the large CPU time required for precise solutions to the scattering problem had hitherto posed a formidable obstacle to such investigations. Despite the enormity of the problem, it is abundantly clear that a significant step in understanding the role of clouds in the general circulation of the atmosphere and climate lies in determining their radiative properties (at least for those clouds whose microphysics is known) on a theoretically precise basis through high-resolution spectral computations. Futher, climate models need to have rigorously trustworthy parameterizations of cloud radiative effects that are calibrated against these benchmark results.

Guided by the ICRCCM precepts and the availability of resources, we have investigated the radiative transfer in an inhomogeneous atmosphere containing water vapor only, cloud only, and vapor plus cloud present simutaneously. The principal characteristic of this study has been the determination of the transfer in an atmosphere containing water vapor and water drops (confined to the 800- to 820-mbar layer) through a rigorous technique that consists of a high spectral resolution (line-by-line) and a multistream, multiple-scattering scheme. All the spectral details of the H_2O molecule (0–17,900 cm^{-1}), as specified in the AFGL data [*Rothman et al.*, 1983], have been taken into account. Although it has been possible to perform the benchmark computations only for two sets of cloud properties owing to the large CPU time involved (Table 1), useful comparisons have been made with the corresponding vapor-only and cloud-only cases. The results confirm the relative radiative effects of water drop vis-a-vis water vapor in the atmosphere that have been pointed out by narrow-band model studies [*Davies et al.*, 1984; *Wiscombe et al.*, 1984]. In particular, the attenuation of solar irradiance in some of the near-infrared frequencies by water vapor above clouds has a substantial impact on the heating rates in the cloud layers.

Our objective of deriving benchmark results for the radiative fluxes and heating rates has also led to the examination of two other numerical techniques that approximate either

TABLE 10. Fraction of Intervals With the Magnitude of the Relative Error in the 800- to 820-mbar Layer Heating Rates ($|\delta_{re}Q|$) Over the Ranges <0.1%, 0.1–1%, and ≥1% Due to the Binning (VC3) Method (Relative to the VC1 or Exact Method)

Width $\Delta\nu$, cm^{-1}	θ_0 = 30° Fraction of Intervals With $\|\delta_{re}Q\|$			θ_0 = 75.7° Fraction of Intervals With $\|\delta_{re}Q\|$		
	<0.1%	0.1–1%	≥1%	<0.1%	0.1–1%	≥1%
	0.60	0.29	0.11	0.67	0.29	0.04
10	0.71	0.18	0.11	0.78	0.18	0.04
50	0.79	0.11	0.10	0.86	0.11	0.03
100	0.79	0.12	0.09	0.87	0.11	0.02
500	0.83	0.11	0.06	0.92	0.08	0
Band	0.90	0.10	0	1.00	0	0
Solar	1.00	0	0	1.00	0	0

The comparisons are analyzed in terms of sums over frequency intervals of uniform width $\Delta\nu$ for the vapor-plus-cloud case. Widths of bands are listed in Table 2, while the width for solar spectrum absorption is 0–18,000 cm^{-1}. Bin parameter N is assumed to be 90 for solar zenith angles (θ_0) of 30° and 75.7°. See section 5.3 for details.

the vapor absorption or the multiple-scattering process. Their accuracy, limitations, and computational resource consumption have been assessed. These nonexact techniques also employ a high spectral (line-by-line) resolution but consume far (at least 25 times) less CPU time than the exact technique. Within the scope of this study, the technique involving the DE approximation is computationally the most efficient method. Over the vapor absorption spectrum (0–18,000 cm^{-1}), it yields a reasonable first-order approximation for the heating rates in the cloud layer when compared to the exact results. However, for the heating rates over smaller frequency intervals (say, hundreds of wave numbers) and for the fluxes in any frequency regime, large errors can occur (>10%).

The method of binning the gas optical depth yields extremely accurate solutions both for the vapor-only and for the vapor-plus-cloud cases. The reasons for the high precision have been investigated in detail for both cases. This method is fast compared to the exact, since it reduces the number of the radiative transfer computations to be performed across the spectrum (the amount of reduction is an arbitrary choice). The findings strongly suggest that this

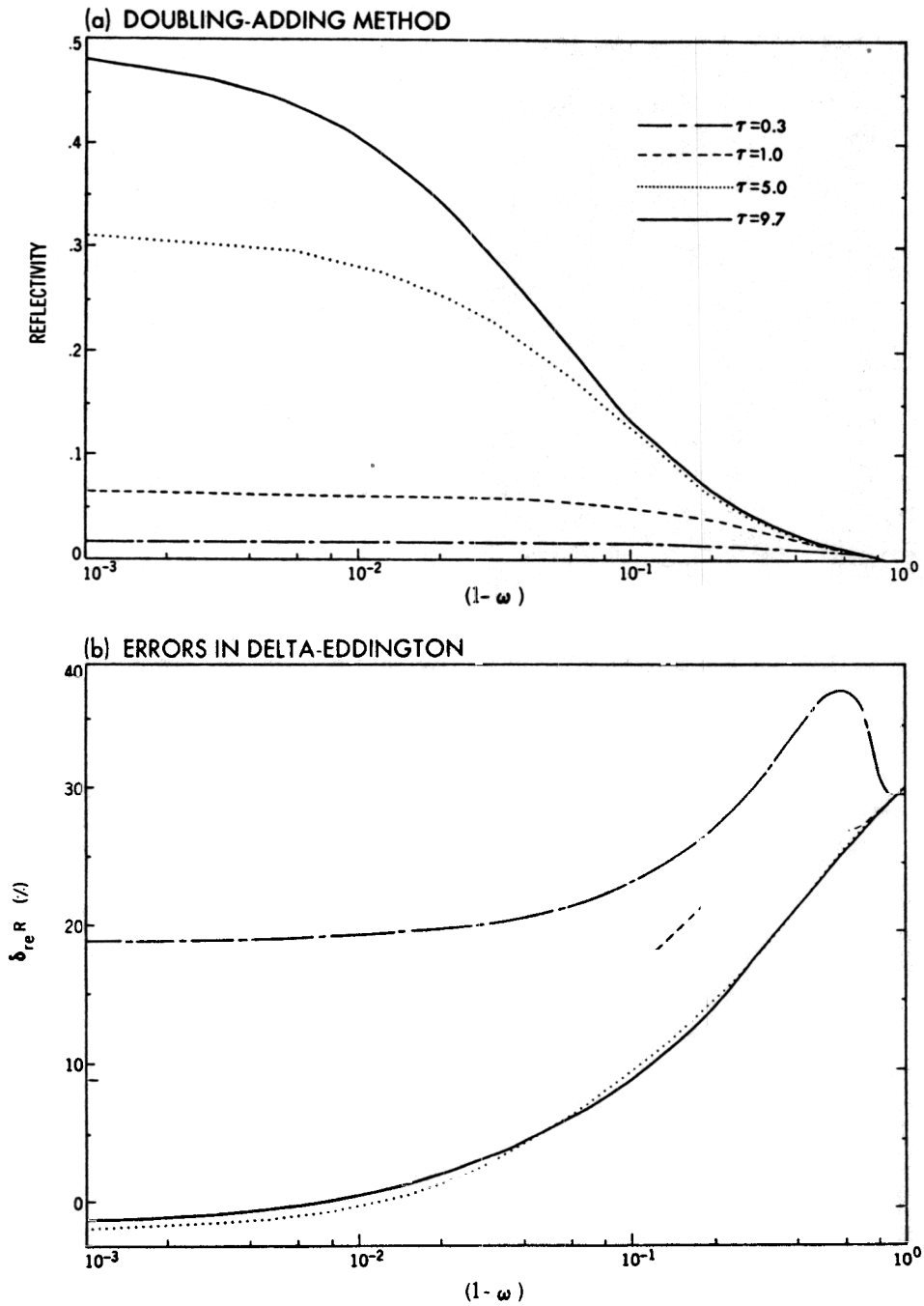

Fig. A1. (*a*) Reflectivity of a cloudy, homogeneous layer with fixed scattering optical depth as a function of layer absorption optical depth (expressed by the single-scattering coalbedo). The computations employ the DA method for cloud scattering optical depths τ of 0.3, 1.0, 5.0, and 9.7, respectively; solar zenith angle is 30°. (*b*) Relative errors obtained by comparing the DE and the DA results as a function of the single-scattering coalbedo.

method can be used to prepare benchmarks for cloudy atmospheres in lieu of the exact technique.

The study of the alternate techniques provides a computationally feasible but still high-spectral-resolution basis for the analyses of a large number of cloud cases (e.g., different optical properties, various altitudes). In the future, clouds occurring in more than one model layer will be considered. This is an even more computationally taxing problem than clouds in a single layer. The CPU time for the exact method increases linearly with the number of layers containing scatterers, so that only the two economical methods discussed here may be feasible at present to investigate the multiple-layer cloud radiative transfer problem in inhomogeneous atmospheres.

APPENDIX: EFFECT OF WATER VAPOR

We examine here the effect of water vapor on the radiative properties of a layer containing cloud drops as computed by the DA and DE methods. The accuracy of the approximation depends on the extinction optical depth and the single-scattering albedo [*King and Harshvardhan*, 1986] of the layer. Given the fine structure in the properties of the H_2O molecule, the radiative properties of a cloudy layer, as computed by approximate methods, can be expected to vary in accuracy over the different monochromatic frequencies. This is demonstrated by considering the reflection and transmission of a homogeneous layer, as obtained by the DA and DE methods, for a wide range of vapor absorption

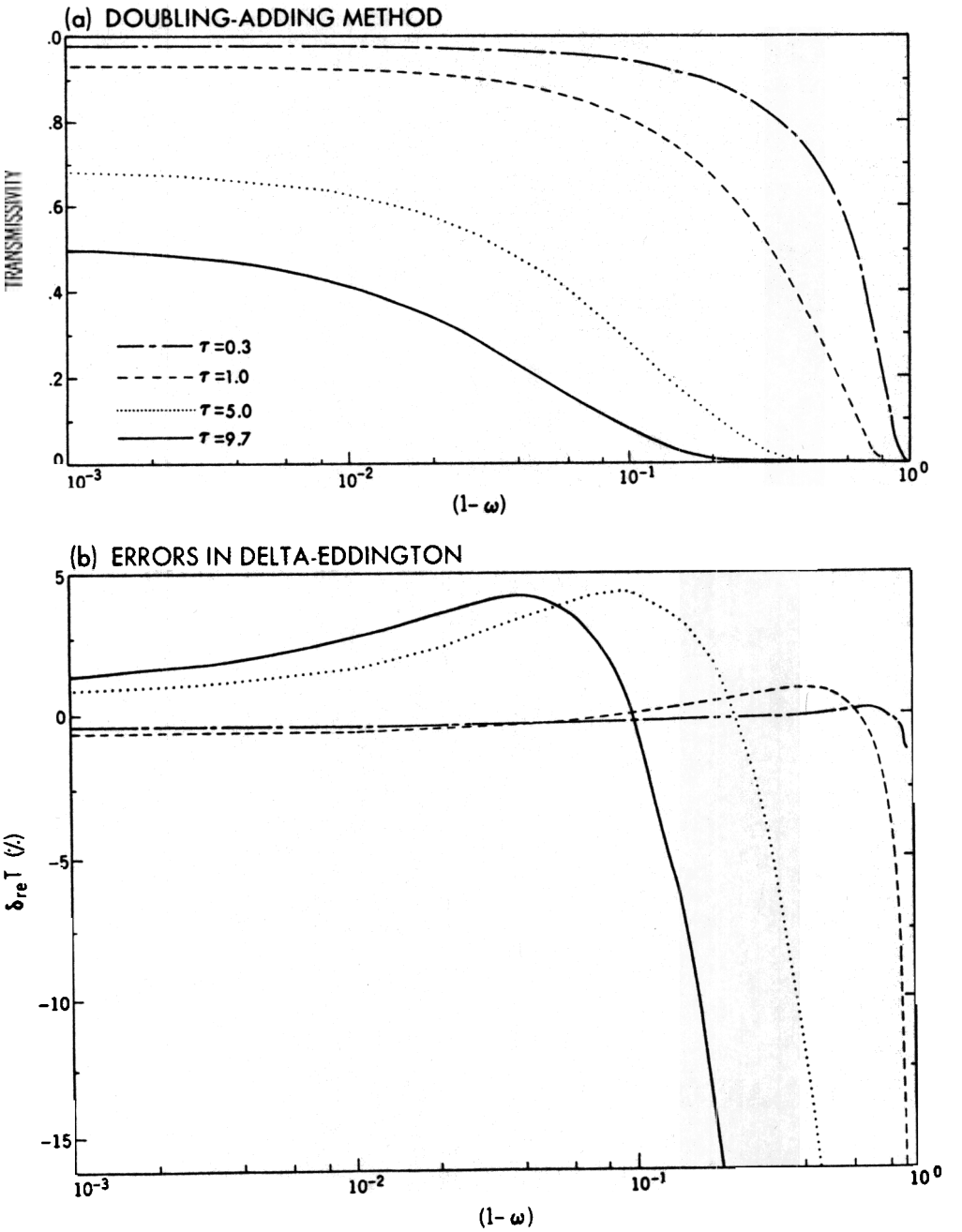

Fig. A2. (*a*) Same as Figure A1*a*, except for the layer transmissivity. (*b*) Same as Figure A1*b*, except for the layer transmissivity.

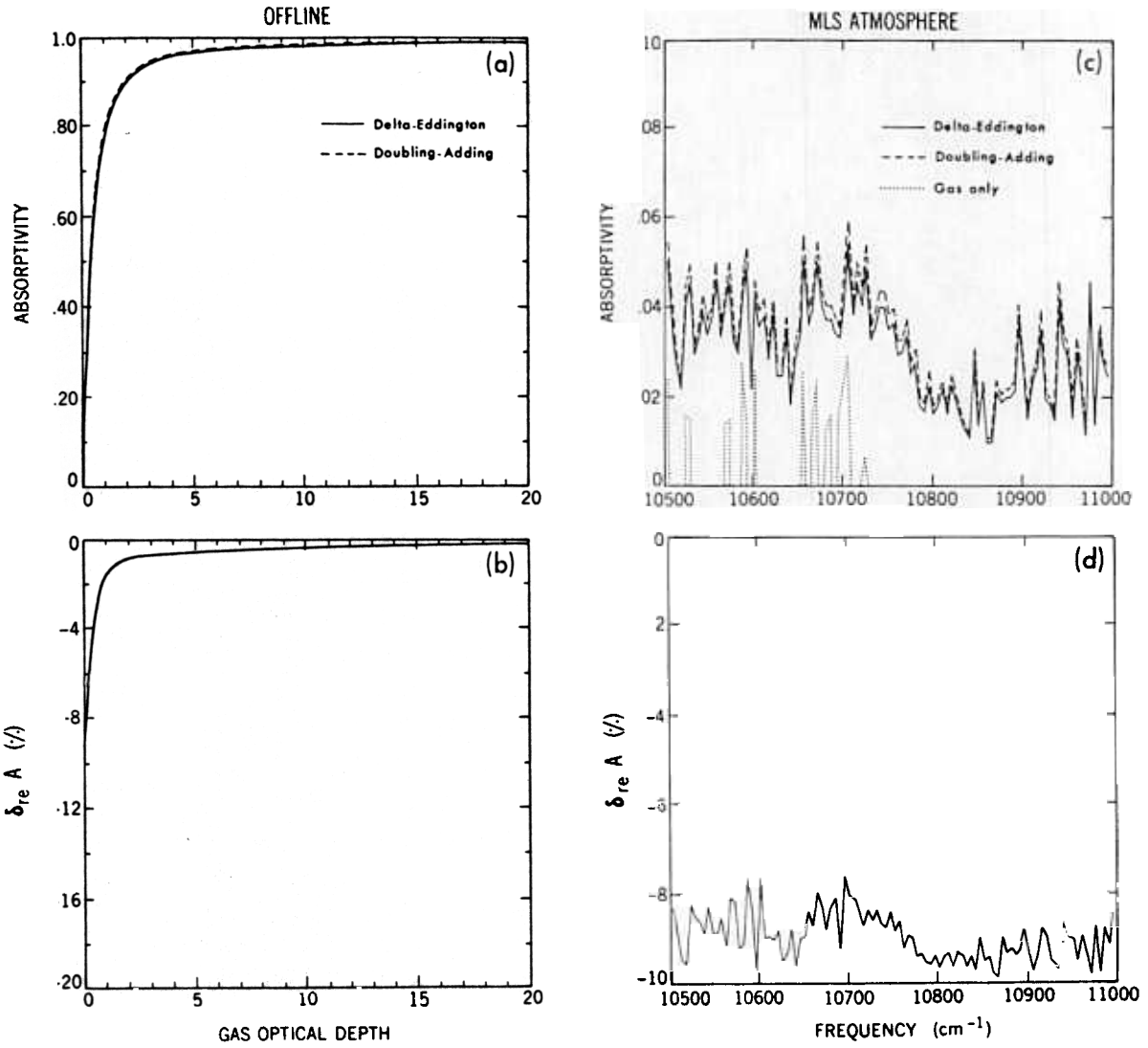

Fig. A3. (*a*) Absorptivity, computed by the DA method, as a function of gas optical depth for a cloudy, homogeneous layer (off-line mode). (*b*) Relative errors due to the DE approximation as a function of gas optical depth. (*c*) Absorptivity as a function of frequency (5 cm^{-1} sums), obtained by employing the DA method for the MLS atmosphere with water vapor. (*d*) Relative error in absorptivity due to the DE approximation over the same frequency regime as shown in Figure A3*c*.

optical depths. The cloud-scattering optical depth is assumed constant. Because vapor optical properties vary on a much finer scale in frequency than do the cloud drop properties, this situation is typical of broad spectral regions in the near infrared. The single-scattering coalbedo $(1 - \omega)$ is selected as a proxy for the vapor absorption optical depth. Cloud drops are assumed to be conservative scatterers whose phase function is represented by the Henyey-Greenstein function (asymmetry parameter is 0.834).

The DA reflectivity (R) of the cloudy layer (CS cloud) is shown as a function of the coalbedo for four different scattering optical depths in Figure A1*a* (solar zenith angle is 30°). Increase in $(1 - \omega)$ denotes an increase in the vapor absorption optical depth, while cloud optical properties are held fixed. The curves thus mimic the influence of spectral variation in the vapor absorption optical depth. The relative error due to the DE approximation ($\delta_{re}R$), as compared with the corresponding DA values in Figure A1*a* for each value of $(1 - \omega)$, is illustrated in Figure A1*b*. Figures A2*a*) and A2*b* are the corresponding illustrations for the transmissivity of the layer (T and $\delta_{re}T$).

Large errors in R occur for smaller scattering optical depths [*Joseph et al.*, 1976; *King and Harshvardhan*, 1986]. Significant relative errors in R and T occur with increasing vapor absorption; however, in this same range the absolute values are small.

The results from Figures A1 and A2 indicate that the radiative properties at any frequency point for any layer where a scatterer is present can suffer considerably in accuracy due to the DE approximation. Further, the relative error of the DE results depends on the optical depth of water vapor. In view of the sharp variation of water vapor optical properties in the near-infrared spectrum, we examine the behavior of the relative error in the radiative properties when considered over several frequency points.

We compare the relative error expected for individual discrete frequency points in a specific interval ("off-line" calculations) with those obtained by averaging the results over a group of such points in the context of a cloud embedded

calculations) with those obtained by averaging the results over a group of such points in the context of a cloud embedded in a layer of the MLS atmosphere model (Figure 1*c*) described in section 2. The results described below constituted a portion of the ICRCCM comparison of exact algorithms for scattering-absorbing inhomogeneous atmospheres. Intercomparisons were made with the results obtained by investigators at NASA-Goddard (Harshvardhan, personal communication, 1989) and excellent agreement was obtained.

The frequency interval considered is 10,500–11,000 cm^{-1}, comprised of ~100,000 frequency points. The cloud is located between 800 and 820 mbar, its optical depth is 9.7, the single-scattering albedo is 0.999718, and the asymmetry factor is 0.834. The cloud single-scattering values are assumed constant in the interval and are approximately similar to those for the ICRCCM CS cloud at the appropriate frequencies.

Figure A3*a* depicts the absorptivity of the layer computed by the DA method in the off-line mode as a funtion of water vapor optical depth. The relative error due to the DE method is shown in Figure A3*b*. In the considered interval, the maximun vapor optical depth is 13, and the relative errors range from −10% to 0%.

The line-by-line results obtained from the DA method for the complete atmosphere are shown in Figure A3*c* with the results being averaged over every 5 cm^{-1}. The absorption in Figure A3*c* is expressed as a fraction of the solar irradiance at the top of the atmosphere (considered to be unity). Figure A3*d* shows the relative errors due to the DE approximation; the errors are confined to between −7% and −10%. This implies that the averaging process has damped out the contributions that may be expected from large gas optical depths and has skewed the values toward the smaller end of the scale, where the off-line results suggest the largest errors. Figure A3*c* also demonstrates the enhancement in the absorption due to the cloud over that by the vapor throughout the frequency interval.

Note: The results discussed in the study have been archived and formatted as sums over 10 cm^{-1}. They will be made available to interested users upon request.

Acknowledgments. We are eternally indebted to Steve Fels for the motivation to undertake this study. His scientific counsel, inspiration, and enthusiasm concerning radiative transfer enabled the successful resolution of the complexities associated with the investigations. We are also grateful to both Steve Fels and Dan Schwarzkopf for providing invaluable suggestions and for their comments on an earlier version of the manuscript. Finally, we acknowledge the support from the GFDL staff in making available the resources to conduct this study.

REFERENCES

Chandrasekhar, S., *Radiative Transfer*, 393 pp., Dover, New York, 1950.

Charlock, T. P., and V. Ramanathan, The albedo field and cloud radiative forcing produced by a general circulation model with internally generated cloud optics, *J. Atmos. Sci.*, *42* 1408–1429, 1985.

Chou, M.-D., Atmospheric solar heating rate in the water vapor bands, *J. Clim. Appl. Meteorol.*, *25*, 1532–1542, 1986.

Coakley, J. A., R. D. Cess, and F. B. Yurevich, The effects of tropospheric aerosols on the Earth's radiation budget; A parameterization for climate models, *J. Atmos. Sci.*, *40*, 116–138, 1983.

Davies, R., W. L. Ridgway, and K.-E. Kim, Spectral absorption of solar radiation in cloudy atmospheres: A 20 cm^{-1} model, *J. Atmos. Sci.*, *41*, 2126–2137, 1984.

Drayson, S. R., Atmospheric transmittance in the CO_2 bands between 12–18 μ, *Appl. Opt.*, *5* , 385–391, 1973.

Fouquart, Y., and B. Bonnel, Computation of solar heating of the Earth's atmosphere: A new parameterization, *Contrib. Atmos. Phys.*, *53*, 35–62, 1980.

Fouquart, Y., and B. Bonnel, and V. Ramaswamy, Intercomparing shortwave radiation codes for climate studies, J. Geophys. Res., this issue.

Hansen, J. E., and L. D. Travis, Light scattering in planetary atmospheres, *Space Sci. Rev.*, *16*, 527–610, 1974.

Harshvardhan, R. Davies, D. A. Randall, and T. G. Corsetti, A fast radiation parameterization for atmospheric circulation models, *J. Geophys. Res.*, *92*, 1009–1016, 1987.

Hunt , G. E., and I. P. Grant, Discrete space theory of radiative transfer and its application to problems in planetary atmospheres, *J. Atmos. Sci.*, *26*, 963–972, 1969.

Joseph, J. H., W. J. Wiscombe, and J. A. Weinman, The delta-Eddington approximation for radiative flux transfer, *J. Atmos. Sci.*, *33*, 2452–2459, 1976.

Kerschgens, M., U. Pilz, and E. Raschke, A modified two-stream approximation for computation of the solar radiation budget in a cloudy atmosphere, *Tellus*, *30*, 429–435, 1978.

King, M. D., and Harshvardhan, Comparative accuracy of selected multiple scattering approximations, *J. Atmos. Sci.*, *43*, 784–801, 1986.

Kratz, D. P., and R. D. Cess, Solar absorption by atmospheric water vapor: A comparison of radiation models, *Tellus*, *37B*, 53–63, 1985.

Labs, D., and H. Neckel, Transformation of the absolute solar radiation data into the international temperature scale of 1968, *Solar Phys.*, *15*, 79–87, 1970.

Lacis, A. A., and J. E. Hansen, A parameterization for absorption of solar radiation in the Earth's atmosphere, *J. Atmos. Sci.*, *31*, 118–133, 1974.

Lenoble, J., Standard procedures to compute the atmospheric radiative transfer in a scattering atmosphere, *IAMAP Publ.*, Int. Assoc. of Meteorol. and Atmos. Phys., Boulder, Colo., 1977.

Liou, K.-N., and G. D. Wittman, Parameterization of the radiative properties of clouds, *J. Atmos. Sci.*, *36*, 1261–1273, 1979.

Luther, F. M., R. G. Ellingson, Y. Fouquart, S. Fels, N. A. Scott, and W. J. Wiscombe, Intercomparison of radiation codes in climate models (ICRCCM): Longwave clear sky results: A workshop summary, *Bull. Am. Meteorol. Soc.*, *69*, 40–48, 1988.

McClatchey, R. A., R. W. Fenn, J. E. A. Shelby, F. E. Voltz, and J. S. Garing, Optical properties of the atmosphere, Rep. *AFCRL-72-0497*, 110 pp., Hanscom Air Force Base, Bedford, Mass., 1972.

Rothman, L. S., R. R. Gamache, A. Barbe, A. Goldman, J. R. Gillis, L. R. Brown, R. A. Toth, J. M. Flaud, and C. Camy-Perot, AFGL atmospheric absorption line parameter compilations: 1982 edition, *Appl. Opt.*, *22*, 2247–2256, 1983.

Schwarzkopf, M. D., and S. B. Fels, The simplified exchange method revisited: An accurate, rapid method for computation of infrared cooling rates and fluxes, J. Geophys. Res., this issue.

Stephens, G. L., Radiation profiles in extended clouds, I, Theory, *J. Atmos. Sci.*, *35*, 2111–2122, 1978.

Twomey, S., Computations of the absorption of solar radiation in clouds, *J. Atmos. Sci.*, *33*, 1087–1091, 1976.

Wiscombe, W. J., On initialization, error and flux conservation in the doubling method, *J. Quant. Spectrosc. Radiat. Transfer*, *16*, 637–658, 1976.

Wiscombe, W. J., and J. W. Evans, Exponential-sum fitting of radiative transmission functions, *J. Comput. Phys.*, *24*, 416–444, 1977.

Wiscombe, W. J., R. M. Welch, and W. D. Hall, The effects of very large drops on cloud absorption, I, Parcel models, *J. Atmos. Sci.*, *41*, 1336–1355, 1984.

S. M. Freidenreich, NOAA Geophysical Fluid Dynamics Laboratory, Princeton, NJ 08542.

V. Ramaswamy, Program in Atmospheric and Oceanic Sciences, Forrestal Campus, Princeton University, P. O. Box 308, Princeton, NJ 08542.

(Received March 8, 1989;
revised November 20, 1989;
accepted January 4, 1990.)